Neurobiology of Disease

Dietary Fiber and Microbiota Metabolite Receptors Enhance Cognition and Alleviate Disease in the 5xFAD Mouse Model of Alzheimer's Disease

Yichen Zhou,[1] Liang Xie,[1,5] Jan Schröder,[2,3,4] Iona S. Schuster,[1,6] Michael Nakai,[5] Guizhi Sun,[2,3,4] Yu B. Y. Sun,[2,3,4] Eliana Mariño,[7] Mariapia A. Degli-Esposti,[1,6] Francine Z. Marques,[5,8] Alexandra Grubman,[2,3,4] Jose M. Polo,[2,3,4] and Charles R. Mackay[1,9]

[1]Department of Microbiology, Monash University, Clayton, Victoria, Australia, 3800, [2]Department of Anatomy and Developmental Biology, Monash University, Clayton, Victoria, Australia, 3800, [3]Development and Stem Cells Program, Monash Biomedicine Discovery Institute, Clayton, Victoria, Australia, 3800, [4]Australian Regenerative Medicine Institute, Monash University, Clayton, Victoria, Australia, 3800, [5]Hypertension Research Laboratory, School of Biological Sciences, Monash University, Clayton, Victoria, Australia, 3800, [6]Center for Experimental Immunology, Lions Eye Institute, Nedlands, Western Australia, Australia, 6009, [7]Department of Biochemistry & Molecular Biology, Monash University, Clayton, Victoria, Australia, 3800, [8]Heart Failure Research Laboratory, Baker Heart and Diabetes Institute, Melbourne, Victoria, Australia, 6009, and [9]School of Pharmaceutical Sciences, Shandong Analysis and Test Center, Qilu University of Technology (Shandong Academy of Sciences), Jinan, China, 6009

Alzheimer's disease (AD) is a neurodegenerative disorder with poorly understood etiology. AD has several similarities with other "Western lifestyle" inflammatory diseases, where the gut microbiome and immune pathways have been associated. Previously, we and others have noted the involvement of metabolite-sensing GPCRs and their ligands, short-chain fatty acids (SCFAs), in protection of numerous Western diseases in mouse models, such as Type I diabetes and hypertension. Depletion of GPR43, GPR41, or GPR109A accelerates disease, whereas high SCFA yielding diets protect in mouse models. Here, we extended the concept that metabolite-sensing receptors and SCFAs may be a more common protective mechanism against Western diseases by studying their role in AD pathogenesis in the 5xFAD mouse model. Both male and female mice were included. Depletion of GPR41 and GPR43 accelerated cognitive decline and impaired adult hippocampal neurogenesis in 5xFAD and WT mice. Lack of fiber/SCFAs accelerated a memory deficit, whereas diets supplemented with high acetate and butyrate (HAMSAB) delayed cognitive decline in 5xFAD mice. Fiber intake impacted on microglial morphology in WT mice and microglial clustering phenotype in 5xFAD mice. Lack of fiber impaired adult hippocampal neurogenesis in both W and AD mice. Finally, maternal dietary fiber intake significantly affects offspring's cognitive functions in 5xFAD mice and microglial transcriptome in both WT and 5xFAD mice, suggesting that SCFAs may exert their effect during pregnancy and lactation. Together, metabolite-sensing GPCRs and SCFAs are essential for protection against AD, and reveal a new strategy for disease prevention.

Key words: Alzheimer's disease; dietary fiber; metabolite-sensing GPCRs

Significance Statement

Alzheimer's disease (AD) is one of the most common neurodegenerative diseases; currently, there is no cure for AD. In our study, short-chain fatty acids and metabolite receptors play an important role in cognitive function and pathology in AD mouse model as well as in WT mice. SCFAs also impact on microglia transcriptome, and immune cell recruitment. Out study indicates the potential of specialized diets (supplemented with high acetate and butyrate) releasing high amounts of SCFAs to protect against disease.

Introduction

Alzheimer's disease (AD), the most common cause of dementia, is characterized by progressive cognitive decline and memory loss (Long and Holtzman, 2019). AD is a global challenge for health and social care; however, currently there is no prevention or treatment that stops or reverses AD cognitive decline. Primary pathologic hallmarks of AD include amyloid precursor protein-derived amyloid-β (Aβ) plaques, intracellular aggregates of hyperphosphorylated tau protein in neurofibrillary tangles, and neuroinflammation (Masters et al., 2015). Mounting evidence shows that the immune system plays a key role in AD, as immune cells, cytokines, inflammasomes, and the complement system are involved in AD pathogenesis (Heneka et al., 2015a,b).

Gut microbiota and microbial metabolites influence various neurologic and neurodegenerative diseases in mouse models, such as multiple sclerosis (Duscha et al., 2020; Kadowaki and Quintana, 2020), epilepsy (Olson et al., 2018), autism spectrum disorder (Sharon et al., 2019), Parkinson's disease (Sampson et al., 2016), and amyotrophic lateral sclerosis (Blacher et al., 2019). The composition of the gut microbiota is also altered in AD mouse models and human AD patients (Harach et al., 2017; Vogt et al., 2017). How the gut microbiota affects these neurologic diseases and their progression is still unclear, especially since the brain is remote from the gut. Short-chain fatty acids (SCFAs) are the major microbial metabolites produced on fermentation of dietary fiber by the gut microbiota. SCFAs dampen immune responses and protect against multiple "Western lifestyle" diseases in mouse models, such as inflammatory bowel disease (Maslowski et al., 2009), asthma (Maslowski et al., 2009; Trompette et al., 2014; Thorburn et al., 2015), Type I diabetes (Mariño et al., 2017b), food allergy (Tan et al., 2016), hypertension and cardiovascular disease (Marques et al., 2017; Kaye et al., 2020), and diabetic nephropathy (Li et al., 2020). SCFAs elicit anti-inflammatory effects by either binding to metabolite-sensing GPCRs, or inhibiting histone-deacetylase (HDAC) activity in human and mice (Koh et al., 2016). Greater adherence to the Mediterranean diet, which is rich in fiber and SCFAs (Davis et al., 2015), is associated with decreased AD biomarkers (Berti et al., 2018), a slower rate of cognitive decline (Morris et al., 2015; Ballarini et al., 2021), and reduced risk of developing AD (Lourida et al., 2013; van de Rest et al., 2015). Collectively, the inflammatory nature of AD (Heneka et al., 2015b), the anti-inflammatory role of fiber, and SCFAs (Thorburn et al., 2014), coupled with human epidemiology, suggest that fiber/SCFAs may protect against AD, and that there is potential to delay or treat AD with novel dietary and microbial approaches.

Here, we report that metabolite-sensing GPCRs are critical in cognition and AD pathology. Lack of fiber or GPR41/43 KO accelerated memory deficits in 5xFAD mice (Oakley et al., 2006), a model of AD, while the use of a high SCFA-releasing diet, diet supplemented with high acetate and butyrate (HAMSAB), protected against cognitive decline. Fiber intake significantly altered gut microbiota composition and gut physiology. We also showed that fiber played a role in microglial morphology and plaque-clustering phenotype, as well as adult hippocampal neurogenesis (AHN). Moreover, HAMSAB feeding significantly altered the transcriptome of microglia at an early stage, which may contribute to pathologic and cognitive changes. Our findings highlight pathways that may underlie AD, the promise of preventing AD using a novel SCFA/dietary approach, and a common thread that connects all "Western lifestyle" diseases studied to date: fiber intake and the gut microbiota, acting through SCFAs and their receptors.

Materials and Methods

Animal model and treatment. Heterozygous 5xFAD mice (B6SJL background) carry mutant human transgenic amyloid precursor protein (Swedish mutation K670/671NL, London mutation V717I, and Florida mutation I716V) and presenilin 1 (PSEN1, M146L and L286V) under the control of the neuron-specific mouse *Thy1* promoter. *Gpr41/43/109a$^{-/-}$*, *Gpr41/43$^{-/-}$*, *Gpr109a$^{-/-}$* WT/5xFAD mice were generated by CRISPR at Monash Genome Modification Platform as described in *Gpr41/43/109a* CRISPR-Cas9 KO. Mouse genotypes from tail biopsies were determined using real-time PCR with specific probes designed for each gene (Transnetyx). Both male and female mice were studied. Mice used in this study are available on request. All mice were housed in an environmentally controlled, specific pathogen-free facility (Monash Animal Research Platform) on a 12 h light-dark cycle, provided with food and water *ad libitum*. All experimental protocols were approved by Monash Animal Ethics Committee (Ethics #17271) and conformed to national and institutional guidelines.

5xFAD mice and WT mice were randomly divided and were fed with different diets: zero fiber diet (Specialty Feeds, SF09-028), control diet (Specialty Feeds, AIN93G), and HAMSAB diet (Specialty Feeds, SF18-086), High-fiber diet (Specialty Feeds, SF11-025), HAMSA (Specialty Feeds, SF18-084), HAMSB (Specialty Feeds, SF17-171). Zero fiber diet does not contain dietary fiber. AIN93G is the control diet with 5% cellulose. HAMSAB diet contains 15% acetylated high-amylose resistant starch, 15% butyrylated high-amylose resistant starch, and 5% cellulose. High-fiber diet contains 9.7% crude fiber and AD fiber, and all CHO as gel crisp starch. HAMSA contains 15% acetylated high-amylose resistant starch and 5% cellulose. HAMSB contains 15% butyrylated high-amylose resistant starch and 5% cellulose.

Gpr41/43/109a CRISPR-Cas9 KO. Gpr41 and Gpr43, Gpr109a, or all three GPCRs were globally knocked out in mice on WT and 5xFAD backgrounds using CRISPR-Cas9 (Monash Genome Modification Platform). The UCSC Genome Browser (https://genome.ucsc.edu/) was used to identify guide RNA target sites flanking the *Gpr109a* gene and *Gpr41/Gpr43* gene. The following guide RNA were used: 95 bp upstream of the ATG of *Gpr109a* (5′-CTGACATGACATAAAGCCGA-3′) and 1282 bp downstream of the STOP codon of *Gpr109a* (5′-TAATC TGTATCCAGCTCGGG-3′) to knock out GPR109a gene; 868 bp upstream of the ATG of *Gpr41* (5′-TACCTGTAACCCAGACGTTA-3′) and 1145 bp downstream of the STOP codon of *Gpr43* (5′-AAGCCAG CTACGGGCTACAC-3′) to knock out both *Gpr41* and *Gpr43* genes. CRISPR RNAs (crRNA, IDT) were annealed with trans-activating crRNA (tracrRNA) to form a functional crRNA:tracrRNA guide RNA

duplex. Cas9 nuclease (IDT, #1081058) was incubated with the guide RNAs to form a ribonucleoprotein complex. Cas9 nuclease (30 ng/μl) and the crRNA:tracrRNA guide RNA duplexes (30 ng/μl) were microinjected into the pronucleus/cytoplasm of the zygotes at the pronuclei stage. Injected zygotes were transferred into the uterus of pseudo pregnant F1 females. Both male and female mice were studied.

Behavioral tests.

• Novel object recognition

The protocol for novel object recognition was adapted from a previous study (Leger et al., 2013). One week before testing, mice were handled 3 times/day at 5 min intervals by the experimenter. Three to four days of handling was performed until mice were well habituated and relaxed. This reduces stress and anxiety from handling, which may interfere with object exploration and recognition (Deacon, 2006). Novel object recognition consists of habituation, a familiarization session, and a test session. Mice were first placed in the empty open field (40 cm L × 40 cm W × 35 cm H, black plastic box without lid) and allowed to explore the open field for 5 min. At 24 h later, two identical objects were placed in the open field, and mice were allowed to explore the two objects freely until 20 s of total exploration time was reached. Exploration was defined when the mouse sniffed the object or touched the objects while looking at it. Sitting and climbing onto the objects or chewing the objects was not considered as exploration. After familiarization, mice were immediately removed and returned to their home cage. One hour later, one of the objects was replaced by a novel object and the test session was performed with the same procedure as the familiarization session. Mice were excluded if they could not reach 20 s exploration time within 10 min in either familiarization session or test session. The open field and objects were cleaned with 70% (v/v) ethanol between animals and between different sessions. Recognition index was calculated for each mouse, which is a reflection for recognition memory. Recognition index = Time (novel)/Time (novel) + Time (familiar). For mice performing multiple novel object recognition tests at different ages, different sets of objects were used. Objects were chosen based on the recommendations of Heyser and Chemero (2012). The two objects have similar size (both can be climbed by the mouse) and odor (odor was minimized by cleaning with 70% (v/v) ethanol), but different shapes, brightness, and texture. For the 5 and 3.5 month novel object recognition test (NOR), a symmetric tower of Lego bricks (6.3 cm H × 3.3 cm L × 3.3 cm W, built in yellow, red, green, blue, black, green brick), and a white bottle with blue bottom (7 cm H × 3 cm L × 3 cm W) were used. For the 6 month NOR, a pink toy bear (5 cm H × 5 cm L × 4 cm W) and an asymmetric Lego tower (5.7 cm H × 5.1 cm L × 5.1 cm W, built in blue, green, yellow, red Lego bricks) were used. For the 8 month NOR, a transparent ball with pink bottom (6 cm H × 4 cm L × 4 cm W) and a pink toy pig (5.3 cm H × 4 cm L × 4.5 cm W) were used. All behavioral tests were performed in the dark phase (active phase between 19:00 P.M. and 23:00 P.M.). To minimize the stress caused by bright lighting, dim lighting illuminated at ~15 lux at the center of the NOR box was used. Mouse behavior was video-recorded using Mi Home Security Camera 360° 1080P (MJSXJ02CM). Data were analyzed manually by an experimenter who was blinded to object novelty and genotype.

• Spontaneous T maze alternation

The protocol for spontaneous T alternation was adapted from previous reports (Deacon et al., 2002; Deacon and Rawlins, 2006). Spontaneous T maze alternation was used to assess the short-term memory of mice. The T maze consisted of one start arm and two goal arms (each arm is 30 cm L × 10 cm W × 20 cm H). A removable central partition (7 cm L × 20 cm H) extended into the start arm. Guillotine doors could close the goal arm entrances from the choice area. The floor was covered with a thin layer of wooden bedding to facilitate running (Deacon et al., 2002). First, the central partition was placed in the T maze, and all guillotine doors were raised. A mouse was placed at the end of the start arm facing away from the goal arms. The mouse was allowed to choose freely between two goal arms. Once the mouse entered a goal arm, the mouse would be confined in the chosen arm for 30 s by closing the guillotine door. After 30 s, the central partition was removed and guillotine doors were all raised, the mouse was returned to the end of the start arm and allowed to choose freely again. The alternation was recorded. Successful alternation was defined as the mouse entering the goal arm that was not visited before. Criteria for entering the goal arm were met when the whole animal, including the tail, entered the goal arm and stayed in the arm for at least 2 s. When an animal immediately left the goal arm after entering, this was not considered as entering. After each trial, any urine or feces were removed before starting the next trial. Mice from the same cage used the same wooden bedding, and the bedding was changed when starting a new cage of mice. Each mouse performed 10 trials over 3 d (four trials on the first day, three trials on the second and third day) with a minimum 30 min interval and the alternation rate was calculated. Alternation rate = number of successful alternations/number of total trials. Any trial that could not be completed within 3 min was aborted. Alternation rate provided an index for short-term memory. All behavioral tests were performed in the dark phase (active phase between 19:00 P.M. and 23:00 P.M.). To minimize the stress caused by bright lighting, dim lighting illuminated at ~15 lux at the center of the T maze was used. The experimenter was blinded to genotype and diet treatment.

Brain immunohistology. Mice were humanely killed by CO_2 asphyxiation, then transcardially perfused with ice-cold PBS. Brains were harvested; left brain hemispheres were dissected and fixed in 4% PFA in PBS overnight at 4°C. Right brain hemispheres were dissected into hippocampus and cortex, followed by immediate freezing in liquid nitrogen and stored at −80°C. Fixed brains were cryoprotected by incubating in 30% (w/v) sucrose solution for 24-48 h at 4°C and then frozen in liquid nitrogen. Frozen brains were stored at −80°C until use. Frozen brains were sectioned into 40- or 20-μm-thick sagittal sections, which were stored in anti-freeze solution (16.7% (w/v) sucrose, 33% (v/v) ethylene glycol, Sigma, #293237) in 0.05 M PB, pH 7.6) at −20°C until use.

Before performing immunofluorescent staining, brain sections were washed 4 times with PBS for at least 15 min at room temperature. Sections were then permeabilized and blocked for 1.5 h in PBST (1 × PBS containing 0.05% (v/v) Tween-20, Biochemicals, #BIO0777) with 0.5% (v/v) Triton X (Sigma, #T9284) and 2% (w/v) BSA (Sigma, #A1470) followed by 1 h incubation with Mouse on Mouse Blocking reagent (Vector Laboratories, MKB-2213, 1:200). Sections were stained with primary antibodies overnight at room temperature. Primary antibodies (diluted in 1% (w/v) BSA and 0.25% (v/v) Triton X) include the following: rabbit anti-Iba-1 (Wako, #019-19741, 1:500), mouse anti-6E10 (Biolegend, #803001, 1:500), rabbit anti-doublecortin (DCX, Cell Signaling, #4604, 1:200). The following day, brain sections were washed 3 times with PBST (10 min each). Then the sections were incubated with secondary antibodies diluted in 1% (w/v) BSA and 0.25% (v/v) Triton X for 2 h at room temperature, including AlexaFluor-488 goat anti-rabbit IgG (H + L) (Invitrogen, #A11008, 1:800), AlexaFluor-568 donkey anti-mouse IgG (H + L) (Invitrogen, #A11037, 1:800). Brain sections were washed once with PBS followed by nuclei staining using DAPI (Invitrogen, D1306; 1:5000 in PBST) for 20 min. After washing, sections were mounted with Mowiol 4-88 mounting medium (Merck Millipore, 475904) and coverslipped. For 6E10 staining, 30 min citrate antigen retrieval was performed before permeabilization and blocking. In brief, the slides are immersed in Target Retrieval Solution (DAKO, #S1699, diluted 1:10 with distilled water) and heated in DAKO PT Link (98°C, #PT20040). The temperature is maintained for 30 min before cooling down. Slides were washed 3 times in PBST before permeabilization and blocking.

Confocal image analysis.

• Microglia morphology, microglia-Aβ clustering analysis

The 25-30 μm z stack images were taken at dentate gyrus (DG) with the 40× oil 1.25 NA objective on Leica SP8 confocal microscope (Leica Application Suite X 3.5.7.23 225) at 2× zoom with 0.37 μm z step size. All images were taken at 1024 × 1024 resolution, resulting in a pixel size

of 142 nm. To quantify microglia morphology, the filament Tracer function from Imaris was used. Microglia were masked with surfaces based on the Iba-1 channel. A starting point was placed at the microglial cell body, and the seed point threshold was adjusted to fill the processes of microglia. The branching structure of microglia was generated by Filament Tracer. The average process length, number of branch points, and number of terminal points for each animal were calculated. All images were quantified with the same parameters. Cell body diameter was measured manually using maximum projection images created in FIJI. Two sagittal brain sections per animal were quantified. The experimenter was blind to diet treatment. All images were quantified with the same parameters.

To quantify the number of microglia clustering around plaques, the spot module from Imaris was used to detect microglia based on the Iba-1 signal, and the surface module was used to construct 3D surfaces of $A\beta$ plaques based on the 6E10 signal. Microglia located within the $20\,\mu m$ threshold from the plaque surface were counted using spots close to surface Xtension. The algorithm measures the distance from the center of the microglia spot to the nearest point of the plaque surface, allowing for the quantification of microglial clustering around plaques. Plaque volume was also measured using surface function. Finally, the number of microglia around the plaque was normalized to plaque volume. To analyze microglial engulfment of $A\beta$, microglia were given a surface based on the Iba-1 channel. 6E10 were masked based on the selected microglia surface. The volume of masked 6E10 was quantified (microglia volume is also recorded) using surface function in Imaris. The volume of engulfed plaque was normalized to microglia volume. Two sagittal brain sections per animal were quantified. All images were quantified with the same parameters. The experimenter was blind to diet treatment.

- $A\beta$ plaque and microglia density

To quantify $A\beta$ plaques and microglia density, $40\,\mu m$ brain sections were stained with 6E10 and Iba-1, images were taken with the $20\times$ oil 0.75 NA objective on Leica SP8 confocal microscope. All images were at 1024×1024 resolution, resulting in a pixel size of 568 nm. Images were taken at the DG and cortex. Plaque % area, plaque size, plaque number, and Iba % area were quantified with FIJI. Two sagittal brain sections per animal were analyzed. All images were quantified with the same parameters. The experimenter was blind to diet treatment.

- DCX$^+$ neuron quantification

To quantify neurogenesis, $40\,\mu m$ brain sections were stained with DCX. The 25-30 μm z stack images were taken from DG with the $20\times$ oil 0.75 NA objective on Leica SP8 confocal microscope with $2\,\mu m$ z step size. All images were at 1024×1024 resolution, resulting in a pixel size of 568 nm. DCX$^+$ neurons were detected using spots function in Imaris. The number of DCX$^+$ neurons were normalized to image z stack steps. Two images were taken from each brain section. Two sagittal brain sections per animal were analyzed. Average number was calculated for each animal. All images were quantified using the same parameters. The experimenter was blind to diet treatment.

Food intake measurement. The food intake was measured for WT and 5xFAD mice at 4 months. Female mice fed zero fiber diet, control diet, and HAMSAB diet were single housed. After 2 d of habituation, daily food intake was measured. In short, food was weighed before giving to the mouse and food was weighed again after 24 h. Food intake was measured for a consecutive 4 d, and average daily food intake was calculated.

Gut histologic analysis. Gut sections were fixed in neutral buffer formalin for 24 h before processing. Fixed gut tissue was processed in Leica PELORIS following a 6 h cycle: formalin 15 min; 80% (v/v) ethanol 15 min; ethanol 15, 15, 15, 30, 45 min; xylene 20, 20, 45 min; paraffin 30, 30, 45 min. The paraffin-embedded gut tissues were sectioned into 4-μm-thick sections and stained with Masson's trichrome and Alcian blue/PAS at Monash Histology Platform.

For Masson's trichrome staining, sections were first placed in Bouin's fixative for 1 h at 60°C. After that, sections were stained in Celestin Blue for 5 min and then in Weigert's hematoxylin for 30 min. Sections were differentiated briefly in acid alcohol before washing in tap water for 10 min. After washing, sections were stained with Biebrich scarlet acid fuchsin for 5 min and applied 5% tungstophosphoric acid for 5 min. Finally, sections were stained with Aniline blue staining solution for 5 min and washed in 1% aqueous acetic acid for 3 min before dehydrating and mounting. Fibrotic areas were in blue, cytoplasm and muscle were in red, while nuclei were in dark brown to black.

For Alcian blue/PAS staining, sections were first incubated in Alcian blue (1% Alcian blue in 3% acetic acid) for 5 min and then oxidized with 1% periodic acid for 10 min. After that, sections were immersed in Schiff's reagent for 15 min and washed thoroughly in water for 10 min. Finally, sections were counterstained in hematoxylin for 30 s and blued in Scott's tap water for 30 s before dehydrating and mounting. Acid mucins are stained in blue and neutral mucins are magenta. Mucin combinations are purple or blue purple depending on the dominant mucin type. Nuclei are dark blue.

Stained sections were imaged with Olympus DotSlide microscope at $20\times$ magnification; all images were taken at 1024×1024 resolution, resulting in a pixel size of 322 nm. ImageJ was used to analyze the images. For gut fibrosis, three $322\,\mu m \times 322\,\mu m$ fields were analyzed for each animal, and the color deconvolution plugin was used to extract fibrotic area. The percent fibrotic area was quantified using the same threshold, and the average fibrotic area was calculated for each animal. To measure villi length in the small intestine, 8 villi from each animal were measured. The average villi length was calculated for each animal. Goblet cells were counted manually by an experimenter blinded to treatment group and genotype. In brief, 8 villi were selected randomly for each animal, and the total number of goblet cells in the villi was counted manually. The number of goblet cells was normalized to the width of the villi.

Cecal DNA extraction, library preparation, and sequencing. Cecal content was collected from 6 month WT mice and 5xFAD mice fed with zero fiber, control, and HAMSAB diet. Cecal contents were frozen immediately in liquid nitrogen after collection. The protocol for library preparation and sequencing was previously described (Jama et al., 2020). In brief, cecal DNA was extracted using QIAamp PowerFecal Pro DNA kit (QIAGEN, #51804) following the manufacturer's instructions. The V4 region of the bacterial 16S rRNA was amplified using previously described PCR methods (Thompson et al., 2017). Briefly, 20 ng of sample DNA was mixed with 515F and 806R primers (Bioneer, 515F forward primer: GTGYCAGCMGCCGCGGTAA, 806R reverse primer: GGACTACNVGGGTWTCTAAT), Platinum Hot Start PCR Master Mix (Fisher Scientific, #13000014) and amplified in a Veriti Thermal Cycler (Fisher Scientific, #4375786) in triplicates. The resulting PCR product was assessed for quality and concentration obtained using the MultiNa MCE-202 Microchip Electrophoresis system (Shimadzu); 240 ng of PCR product per sample was pooled and purified using the PureLink PCR Purification Kit (Fisher Scientific, #K310002). Samples were sequenced in Illumina MiSeq Sequencer (300 bp paired end reads) at the Australian Genome Research Facility.

Microbiome data analysis. Sequenced data in the form of FASTQ files were obtained from the sequencing facility and passed initial quality control using FASTQC version 3 (available from: https://www. bioinformatics.babraham.ac.uk/projects/fastqc/). QIIME2 (version 2019-10) workflow was used for downstream analysis (Bolyen et al., 2019). Raw reads were first trimmed (to ensure the quality of at least 50% of reads were >20 Phred score). Reads were then merged, dereplicated, and chimeric reads were removed. DADA2 QIIME2 plugin was used to denoise the reads (Callahan et al., 2016). The Greengenes database (gg-13-8-99-515-806-nb-classifier.qza) was used as a classifier for all taxonomy-related plots and tables (DeSantis et al., 2006). The α-diversity rarefaction curves using the Shannon Index were generated to determine the ideal sequencing depth for further analyses. A minimum sampling depth of 9980 annotated sequence variants was used.

Both qualitative (Jaccard and unweighted UniFrac distance) and quantitative (Bray-Curtis dissimilarity and weighted UniFrac

distance) were used to determine β-diversity. The permutational ANOVA (PERMANOVA, 999 permutations for pseudo-F distribution) was performed to test the separation between groups. $p < 0.05$ was considered significant. p values were Bonferroni-corrected for multiple testing, where false discovery rate $q < 0.05$ was considered significant.

SCFA analysis. The protocol for SCFA analysis was previously described (Yap et al., 2021). Perfused brain samples were stored at −80 until processing. Acetate and butyrate were measured by gas chromatography after liquid-liquid extraction. SCFAs were directly measured after solvent extraction using specialized polar phase gas chromatography-mass spectrometry Phenomenex Zebron ZBFFAP column (Phenomenex); 100 µg of brain samples was mixed with internal standards (50 µl of 200 µM heptanoic acid), and then transferred into glass test tubes containing 30 µl of 0.2 M NaOH. Samples were mixed vigorously with 3 ml of diethyl ether, and then centrifuged for 5 min, and left at room temperature until the upper ether layer was removed. The residue was redissolved in cold 30 µl of 1 M phosphoric acid in a glass insert GC vial. Samples were analyzed on an Agilent 7890A gas chromatograph (Agilent Technologies). Peaks were detected with a flame ionization detector at 210°C and identified and quantitated against calibration standards. Intra-assay CVs were 14.2% and 10.3% for sodium acetate and sodium butyrate, respectively.

Ex vivo microglia isolation. The protocol for *ex vivo* microglia isolation was previously described (Grubman et al., 2021). Mice were transcardially perfused with ice-cold PBS, and brains were harvested (cerebellum and olfactory bulb were excluded). Single-cell suspensions were prepared by mechanical dissociation in Dounce buffer (15 mM HEPES, 0.5% (w/v) glucose in HBSS, Invitrogen, 14175095) followed by filtering through 70 µm mesh. Single-cell suspensions were washed with Dounce buffer and centrifuged at 850 × g for 5 min at 4°C. Cell pellets were resuspended in 6 ml 70% (v/v) isotonic Percoll in PBS (isotonic Percoll: 1:9 ratio of 10× PBS to Percoll, Sigma-Aldrich, P4937), overlaid with 6 ml 37% (v/v) isotonic Percoll in PBS. Percoll gradient was centrifuged at 2000 × g for 25 min at 4°C with no brake. After spinning, cells were harvested from 37% 70% Percoll interphase and washed in PBS. The cells were incubated with anti-mouse Fc block (BD Biosciences, 553141; 1:200) for 10 min and stained with CD11b-PECy7 (Biolegend, 101216; 1:200), CD45-BV786 (BD Biosciences, 564225; 1:100), and CX3CR1-FITC (Biolegend, 149020; 1:100) for 30 min on ice. Propidium iodide (PI, Sigma-Aldrich, 1:500) was added to the cells before sorting to distinguish live and dead cells. Fc block, antibodies, and PI used in this protocol were diluted in FACS buffer (0.5% (w/v) BSA, 2.5 mM EDTA in PBS). Microglia were sorted using FACSAria III cell sorter (BD FACSDiva Software version 8.0.1). Microglia were gated as singlets → viable cells (PI$^-$)→ CD11b$^+$, CD45^{low}→CX3CR1$^+$.

Microglial RNA-seq. RNA extraction, library preparation, and RNA-seq were previously described (Grubman et al., 2021). RNA extraction from 1×10^5 to 4×10^5 microglia was performed on QIAcube (QIAGEN) using the RNeasy Micro Kit (QIAGEN, #74004). The quality of RNA was determined using Bioanalyser (Agilent RNA 6000 Pico kit, #5067-1513); 0.5-2 ng of RNA samples with RIN value > 8 was selected for library preparation. An 8 bp sample index and a 10 bp unique molecular identifier were added during initial poly (A) priming. Twenty-four RNA samples were multiplexed (23 microglia samples and 1 iPSC control for normalization for one run, totally two runs with 46 microglia samples and 2 iPCS control). Pooled samples were amplified using a template switching oligonucleotide. The Illumina P5 (5′ AAT GAT ACG GCG ACC ACC GA 3′) and P7 (5′ CAA GCA GAA GAC GGC ATA CGA GAT 3′) sequences were added by PCR and Nextera transposase, respectively. The library was designed so that the forward read (R1) utilizes a custom primer (5′ GCC TGT CCG CGG AAG CAG TGG TAT CAA CGC AGA GTA C 3′) to sequence directly into the index and then the 10 bp unique molecular identifier. The reverse read (R2) uses the standard R2 primer to sequence the cDNA in the sense direction for transcript identification. The library pools were with a mean size of ∼330 bp at a concentration of ∼3 nM. Following denaturation, 1.6 pM of library pools was sequenced on the NextSeq550 (Illumina), using the NSQ V2.5 High output kit (Illumina # 20024906) in accordance with the Illumina Protocol 15046563 version 02, generating 2 reads per cluster

composed of a 19 bp forward read and 72 bp reverse read. Quality control, library preparation, and sequencing were performed at the MHTP Medical Genomics Facility by Trevor Wilson.

RNA-seq analysis. Sequencing reads were mapped to the mouse transcriptome reference genome (GRCm38) using STAR (version 020201). We then established read counts for each gene using featureCounts (version 1.5.2). We analyzed the bulk RNA-seq read counts using R (version 3.6.3) and limma (version 3.42.2), and edgeR (version 3.28.1). Data handling and plotting were performed using tidyverse (version 1.3.0). We first removed lowly or nonexpressed genes by requiring a log2 CPM count of >1 in at least 3 samples. Next, we calculated TMM normalization factors to remove composition bias using calcNormFactors. We established the sample S2830 as an outlier and removed it from further analysis. To visualize dimensionality reduction of the sequencing data, we first removed unwanted variation in the data with removeBatchEffect and selected sample sex and age to be regressed out from the CPM values of the read counts. The multidimensional scaling plot used plotMDS and ggplot2 to visualize the remaining variance in the data. To determine differentially expressed genes (DEGs), we first determined the gene-wise variance trends using voom. Then, we built a linear model with the lmFit function and genotype, diet, age, and sex as covariates. We also analyze the data with the diet modeled as a continuous variable (1, zero fiber; 2, control; 3, HAMSAB) alongside sample age and sex. The diet-specific DEGs are visualized in a heatmap (using the pheatmap function, version 1.0.12), after creating normalized read counts with above described modeling and the removeBatchEffect function. We further tested the diet contrast for enrichment of disease-associated microglia (DAM) signature genes using the roast function and the same design matrix as for the continuous diet DEG analysis. Additionally, we visualized those gene sets as volcano plots by using the diet contrast's log fold change and adjusted p value results from the topTable function and the limma results from above.

Retro-orbital intravenous CD45 labeling. Mice were anesthetized with isoflurane by inhalation. Under deep anesthesia, retro-orbital intravenous injection of 2.5 µg PECy7-labeled anti-CD45 antibody (BD Biosciences, #552848, diluted in 200 µl DPBS) was performed using a 27G insulin syringe (Terumo, #SS05M2713KA). Mice were allowed to regain consciousness before being humanely killed by CO_2 asphyxiation 3 min after injection.

Flow cytometry for brain. Mice were humanely killed by CO_2 asphyxiation. Brains were harvested and collected into cold PBS (cerebellum and olfactory bulb were excluded). Brain tissue was finely minced in 500 µl digestion buffer (1% (v/v) DNase I (Merck, D4527-40KU) and 1% (w/v) collagenase IV (Invitrogen, 17104019) in 1× PBS and digested for 30 min at 37°C. Digested tissue was mechanically disrupted, filtered through 70 µm mesh, and enriched for leukocytes by Percoll (Sigma, GE17-0891-01). In short, the brain pellet was resuspended in 4 ml of 30% (v/v) Percoll (diluted in PBS) and was layered onto 4 ml of 70% (v/v) Percoll (diluted in PBS). Percoll gradient was centrifuged at 900 × g for 20 min at 20°C with no acceleration and brake. After spinning, cells were harvested from the interphase and washed in the FACS buffer. Single-cell suspensions were counted before labeling dead cells with fixable viability dye FVS620 (BD Biosciences, #564996, 1:1000) for 15 min on ice. Nonspecific binding was blocked using mouse FcR blocking reagent (Miltenyi Biotec, #130-092-575, 1:50) for 10 min on ice before proceeding to surface marker staining. Cells were stained with surface marker-specific antibodies for 30 min on ice and fixed and permeabilized with Foxp3/ Transcription factor Staining Buffer Set (eBioscience, #00-5523-00) followed by FoxP3 staining. Data were acquired on a BD FACSymphony A3. The flow cytometry staining panel included KLRG1- BUV395 (BD Biosciences, #740279,1:100), CD11c-BUV496 (BD Biosciences, #750483, 1:200), NK1.1-BV421 (BD Biosciences, #562921 1:100), CD69-BUV563 (BD Biosciences, #741234, 1:50), CD4-BUV661 (BD Biosciences, #612974, 1:200), CD8-BUV737 (BD Biosciences, #612759, 1:200), CD11b-BUV805 (BD Biosciences, #741934, 1:400), MHC II-BV510 (BD Biosciences, #742893, 1:100), Ly6C-BV570 (Biolegend, #128030, 1:200), Ly6G-BV605 (BD Biosciences, 563005, 1:100), F4/80-BV711 (BD Biosciences, 565612, 1:100), CD19-BV786 (BD Biosciences, 563333,1:200), FoxP3-AF488 (Biolegend, #320012, 1:100), CD3-PerCPCy5.5 (BD Biosciences, #551163,

1:100), TCRβ-PerCPCy5.5 (BD Biosciences, #560657, 1:100), CD115-APC (Biolegend, #135510, 1:200), MHC II-PE (Biolegend, #107608, 1:1000), and CD45.2-APCCy7 (BD Biosciences, #560694, 1:100).

Statistical analysis. No statistical methods were used to predetermine sample sizes, but the sample sizes were determined based on similar, previously conducted studies (Choi et al., 2018; Lourenco et al., 2019; Martorell et al., 2019). Animals were randomized into different groups with comparable numbers of animals in each group whenever possible. Datasets were assessed for normality and group variance using the Shapiro–Wilk normality test before statistical testing. All analyses were performed with Prism 9 (GraphPad). Values are expressed as mean ± SEM unless otherwise stated. Specific statistical parameters are detailed in the figure legends.

Data availability statement. 16S rRNA-seq: https://dataview.ncbi. nlm.nih.gov/object/PRJNA770817?reviewer=m7gtk382nagnes3hcnsnar70fr. Microglial RNA-seq: To review GEO accession GSE186210: https://www. ncbi.nlm.nih.gov/geo/query/acc.cgi?acc=GSE186210.

Code availability statement. Code is available from the authors by reasonable request.

Results

A role for metabolite-sensing GPCRs in AD pathogenesis

SCFAs signal through metabolite-sensing GPCRs (Koh et al., 2016), including GPR41, GPR43, and GPR109A. In animal models, these receptors have been shown to be relevant in the physiopathological mechanisms of several Western-associated diseases (Thorburn et al., 2014; Macia et al., 2015; Tan et al., 2016). Therefore, we hypothesized that they may also be important in AD. To test this, we generated global single, double, and triple *Gpr41*, *Gpr43*, and *Gpr109a* KO mice in WT and 5xFAD background (Oakley et al., 2006), and performed an NOR assessing recognition memory (Leger et al., 2013). Deletion of these receptors produced a striking phenotype analyzed with two-way ANOVA and Tukey's multiple comparison test. GPCR genotype significantly contributes to recognitive index ($F_{(3,92)} = 10.32$, $p = 6.3 \times 10^{-6}$); however, AD genotype did not have a significant effect on cognition ($F_{(1,92)} = 3.154, p = 7.9 \times 10^{-2}$); also, there is no interaction between GPCR genotype and AD genotype ($F_{(3,92)} = 0.668$, $p = 0.57$). *Gpr41/43/109a*$^{-/-}$ 5xFAD mice showed 21.2% lower recognition index (Fig. 1a, $p = 0.016$) and *Gpr41/43*$^{-/-}$ 5xFAD showed 24.2% lower recognition index (Fig. 1a, $p = 0.024$) compared with *Gpr41/43/109a*$^{+/+}$ 5xFAD mice at 5 months. *Gpr109a* was not required for recognition memory in 5xFAD mice (Fig. 1a). Strikingly, *Gpr41/43/109a*$^{-/-}$ WT mice also showed significant cognitive deficits (Fig. 1a, 25.7% lower recognition index compared with *Gpr41/43/109a*$^{+/+}$ WT mice, $p = 0.0029$). Thus, *Gpr41* and *Gpr43* play an important role in cognition and memory in AD mice.

Next, we examined Aβ plaque load, one of the major pathologic markers in AD (Masters et al., 2015), in GPCR KO mice. We quantified the number and size of Aβ plaque and analyzed with two-way ANOVA followed by Tukey's multiple comparison test. GPCR genotype have a significant effect on plaque number ($F_{(3,70)} = 4.495$, $p = 6 \times 10^{-3}$) and plaque size ($F_{(3,70)} = 10.47$, $p = 8 \times 10^{-6}$). Also, DG and cortex have significantly different number of plaques ($F_{(1,70)} = 21.73, p = 1.4 \times 10^{-5}$). Mice lacking GPCRs had more and larger Aβ plaques (Fig. 1b-d). For example, *Gpr41/43/109a*$^{-/-}$ 5xFAD mice had 145.4% more plaques ($p = 0.0159$), and the plaques were 47.1% bigger ($p = 0.002$) than *Gpr41/43/109a*$^{+/+}$ 5xFAD mice in the cortex (Fig. 1b-d). Lack of metabolite-sensing GPCRs did not affect plaque number but increased plaque size in the DG (Fig. 1c,d). Thus, metabolite-sensing GPCRs may be required for optimal Aβ plaque clearance. We then evaluated the state of the microglia, as they are

involved in AD pathogenesis (Gosselin et al., 2017; Hansen et al., 2018). We stained the brain slices with Iba1, a microglia marker, and quantified Iba1$^+$ area. The data were analyzed with two-way ANOVA followed by Tukey's multiple comparison. AD genotype significantly contributed to Iba1$^+$ % area in the cortex ($F_{(1,70)} = 57.48$, $p < 1 \times 10^{-6}$) and DG ($F_{(1,70)} = 21.13$, $p = 1.8 \times 10^{-5}$). GPCR KO mice showed higher microglial density in the cortex and DG (Extended Data Fig. 1-1b,c), for example, *Gpr41/43*$^{-/-}$ 5xFAD mice had significantly higher microglia density in cortex ($p = 7.5 \times 10^{-3}$) and DG ($p = 7.3 \times 10^{-3}$). However, we observed no difference in microglial morphology (Extended Data Fig. 1-1d-g) and microglial clustering (Extended Data Fig. 1-1h) between GPCR KO mice and *Gpr41/43/109a*$^{+/+}$ mice. Finally, as AHN has been shown to be closely associated with cognition in physiology and disease (Costa et al., 2015), we examined whether GPCRs influenced AHN by quantifying DCX expressing neurons in the DG, and the results were analyzed with two-way ANOVA followed by Tukey's multiple comparison. AD genotype ($F_{(1,73)} = 24.56$, $p = 4 \times 10^{-6}$) and GPCR genotype ($F_{(3,73)} = 6.196$, $p = 8 \times 10^{-4}$) had a significant effect on the number of DCX$^+$ neuron, and there is no interaction between AD genotype and GPCR genotype ($F_{(3,73)} = 0.5489$, $p = 0.65$). *Gpr41/43/109a*$^{-/-}$ 5xFAD mice had 41.5% less DCX$^+$ neurons than *Gpr41/43/109a*$^{+/+}$ 5xFAD mice (Fig. 1e,f, $p = 0.021$). Similar results were observed in WT mice (Fig. 1e,f). Together, these data indicate that metabolite-sensing GPCRs are key regulators for Aβ plaques and microglia density in 5xFAD mice, and play an important role in AHN in both AD and WT mice.

Dietary fiber improves cognition and memory in mice

GPR41 and GPR43 are exclusively activated by dietary fiber-derived metabolites, the SCFAs, and our previous studies in other diseases have phenocopied GPCR KOs using low or zero fiber diets (Macia et al., 2015). Thus, the effect of GPR41 and GPR43 on cognition and pathology strongly implicated a role for fiber and SCFAs in AD pathogenesis. To test this, we fed 5xFAD mice and WT mice diets releasing different amounts of SCFAs and performed a series of cognitive tests, including NOR at 5, 6, and 8 months, and spontaneous T maze alternation testing of spatial working memory (Deacon and Rawlins, 2006) at 6 and 8 months (Fig. 2a). All behavioral test data were analyzed with two-way ANOVA followed by Tukey's multiple comparison. The diets include zero fiber diet (contains no dietary fiber), AIN93G (a standard mouse diet with fiber in the form of 5% cellulose), and HAMSAB diet (Mariño et al., 2017b) (AIN93G supplemented with 15% HAMSA and 15% HAMSB). All three diets contain similar levels of digestible energy (zero fiber diet: 16.9 MJ/kg, control diet: 16.1 MJ/kg, HAMSAB diet: 16.3 MJ/kg). The micro- and macro-nutrients are shown in Table 1. 5xFAD mice and WT mice fed either zero fiber or HAMSAB diet showed reduced body weight compared with mice fed control diet at 6 months (Extended Data Fig. 2-1a,b). To determine whether reduced body weight was because of altered food intake, we measured daily food consumption at 4 months. Curiously, WT mice and 5xFAD mice fed HAMSAB diet consumed more food compared with mice fed control diet, and WT mice and 5xFAD mice fed zero fiber diet showed similar food consumption compared with mice fed control diet (Extended Data Fig. 2-1c), suggesting that food intake did not affect body weight.

HAMSAB feeding has been reported to result in very high levels of peripheral acetate and butyrate in mice (Mariño et al., 2017a). In our study, HAMSAB feeding significantly increased
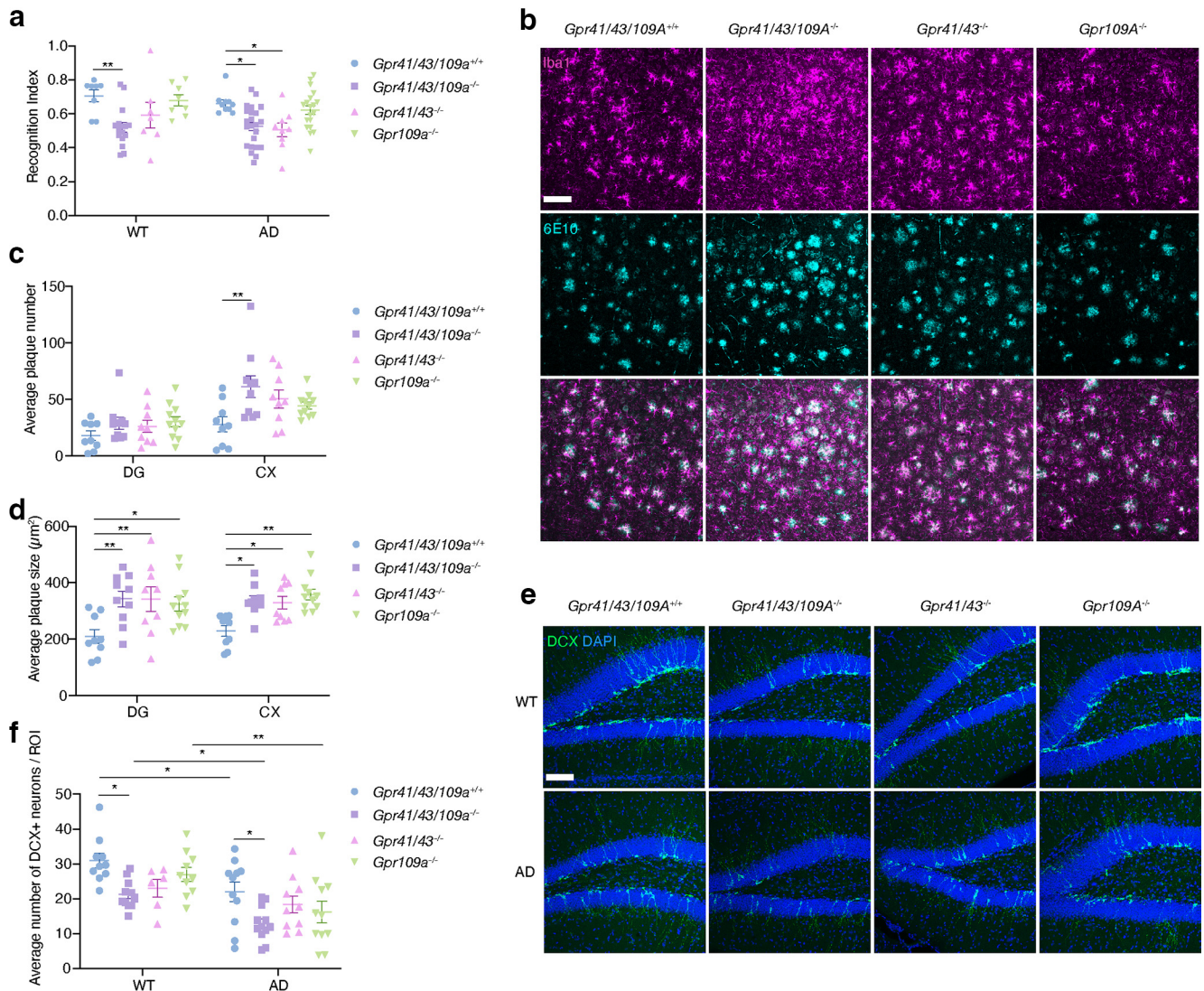
Figure 1. GPR41 and/or GPR43 play an important role in cognition and pathology. ***a***, Recognition index of NOR test of 5 month *Gpr41/43/109a*[+/+], *Gpr41/43/109a*[−/−], *Gpr41/43*[−/−], *Gpr109a*^{−/−} WT/5xFAD mice (WT *Gpr41/43/109a*[+/+] $n = 8$, WT *Gpr41/43/109a*[−/−] $n = 16$, WT *Gpr41/43*[−/−] $n = 7$, WT *Gpr109a*^{−/−} $n = 8$, AD *Gpr41/43/109a*[+/+] $n = 10$, AD *Gpr41/43/109a*[−/−] $n = 23$, AD *Gpr41/43*[−/−] $n = 9$, AD *Gpr109a*^{−/−} $n = 19$). ***b***, Representative immunofluorescence images of Iba1^{+} microglia (magenta) and 6E10[+] plaques (cyan) from the cortex of 6 month *Gpr41/43/109a*[+/+], *Gpr41/43/109a*[−/−], *Gpr41/43*[−/−] mice, *Gpr109a*^{−/−} 5xFAD mice. Scale bar, 100 μm ***c***, ***d***, Average plaque number (***c***) and plaque size (***d***) in DG and cortex. AD *Gpr41/43/109a*[+/+] $n = 9$, AD *Gpr41/43/109a*[−/−] $n = 10$, AD *Gpr41/43*[−/−] $n = 9$, AD *Gpr109a*^{−/−} $n = 11$. ***e***, ***f***, Representative immunofluorescence images (***e***) and quantification (***f***) of DCX[+] newly born neurons (green) from the DG of 6 month *Gpr41/43/109a*[+/+], *Gpr41/43/109a*[−/−], *Gpr41/43*[−/−] mice, *Gpr109a*^{−/−} 5xFAD mice. Scale bar, 100 μm. WT *Gpr41/43/109a*[+/+] $n = 10$, WT *Gpr41/43/109a*[−/−] $n = 11$, WT *Gpr41/43*[−/−] $n = 6$, WT *Gpr109a*^{−/−} $n = 10$, AD *Gpr41/43/109a*[+/+] $n = 11$, AD *Gpr41/43/109a*[−/−] $n = 12$, AD *Gpr41/43*[−/−] $n = 10$, AD *Gpr109a*^{−/−} $n = 11$. Data are mean ± SEM. *$p < 0.05$, **$p < 0.01$; two-way ANOVA and Tukey's multiple comparison test. Extended Data Figure 1-1 supports Figure 1.

the level of acetate and butyrate in the brain compared with control and zero fiber diets (Fig. 2*b*,*c*) as analyzed by two-way ANOVA followed by Tukey's multiple comparison. Diet had a significant effect on acetate level ($F_{(2,49)} = 18.95$, $p < 1 \times 10^{-6}$) and butyrate level ($F_{(2,42)} = 8.84$, $p = 6 \times 10^{-3}$), indicating that SCFAs can travel from the gut to the brain. AD genotype did not significantly contribute to SCFA level, and there is no interaction between diet and genotype. We started feeding the diets from embryonic day 0.5 (E0.5), to capture any possible developmental effects that might be contributing to disease, and pups were weaned onto the same diet as their mother (Fig. 2*a*).

As previous studies reported that dietary fiber modulates the gut microbiota in various disease models (Trompette et al., 2014; Macia et al., 2015; Mariño et al., 2017a; Kaye et al., 2020), we analyzed the gut microbiota from 5xFAD mice and WT mice by 16S ribosomal RNA (rRNA) sequencing.

HAMSAB intake significantly influenced β diversity as revealed by unweighted and weighted Unifrac distances (Extended Data Fig. 2-2*c*,*d*). Neither genotype nor sex significantly contributed to the variation, suggesting that diet is the most significant factor driving microbiome differences. At phylum level, diet significantly contributed to *Bacteroidetes* abundance ($F_{(2,63)} = 36.73$, $p < 1 \times 10^{-4}$) and *Cyanobacteria* abundance ($F_{(2,63)} = 38.66$, $p < 1 \times 10^{-4}$) when analyzed with two-way ANOVA followed by Tukey's multiple comparison test. HAMSAB diet significantly enriched *Bacteroidetes* ($p = 1 \times 10^{-3}$) and *Cyanobacteria* ($p = 2.6 \times 10^{-3}$) in 5xFAD mice compared with control diet, while the gut microbiota of zero fiber and control groups were dominated by Firmicutes in 5xFAD mice (Extended Data Fig. 2-2*e*). Similar microbiome composition was also observed in WT mice. Specifically, HAMSAB diet enriched multiple SCFA-producing bacteria (Koh et al., 2016), such as
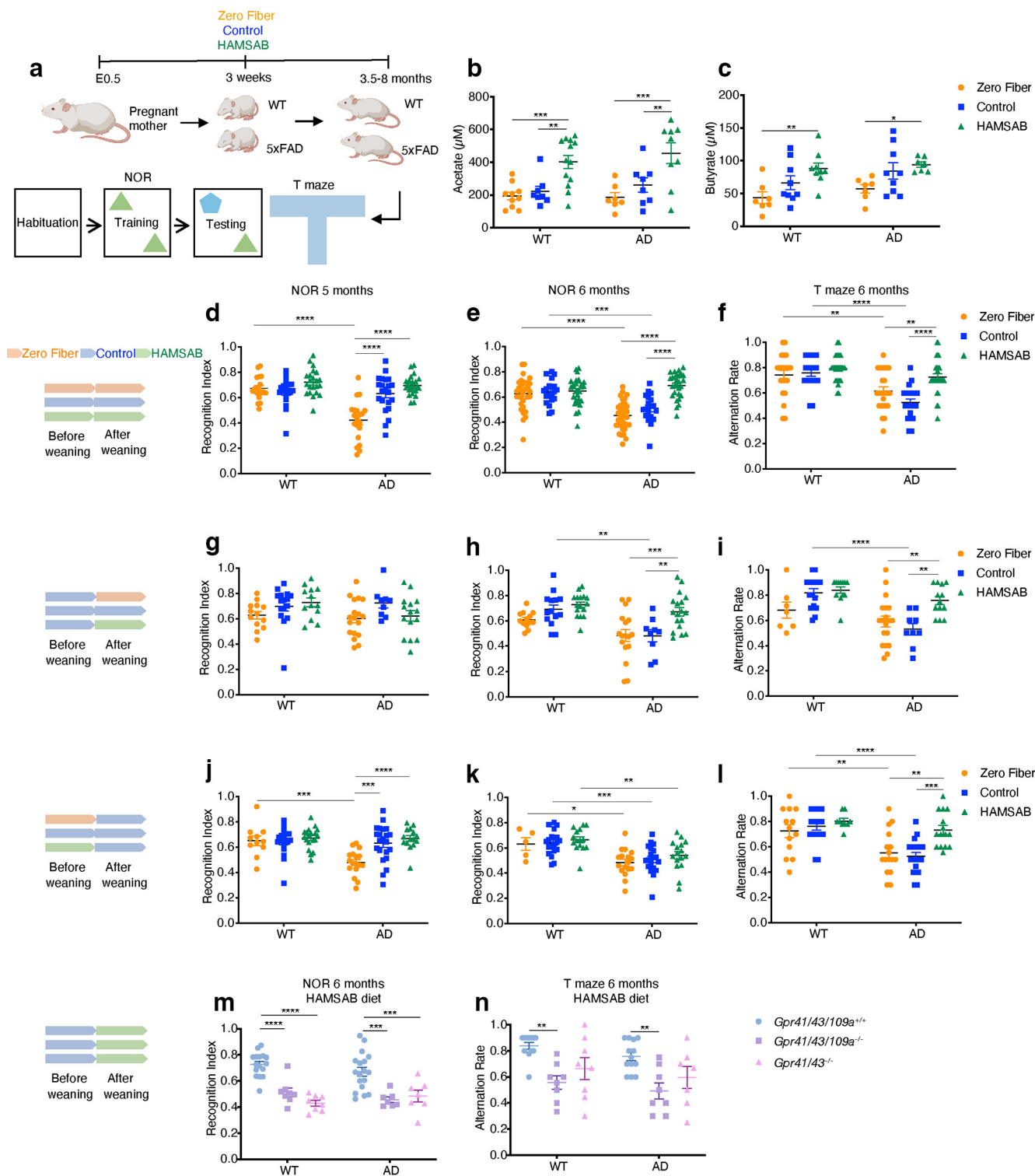
Figure 2. Dietary fiber improves cognitive function. **a**, Schematic of experimental design created with Biorender.com. **b**, **c**, Concentration of acetate (**b**) and butyrate (**c**) in the brains of 6 month WT and 5xFAD mice fed zero fiber, control, HAMSAB diet (acetate: WT zero fiber $n = 10$, WT control $n = 8$, WT HAMSAB $n = 13$, AD zero fiber $n = 7$, AD control $n = 8$, AD HAMSAB $n = 9$; butyrate: WT zero fiber $n = 7$, WT control $n = 9$, WT HAMSAB $n = 9$, AD zero fiber $n = 7$, AD control $n = 9$, AD HAMSAB $n = 7$). **d**, **e**, Recognition index of NOR test of 5 month (**d**) and 6 month (**e**) WT mice and 5xFAD mice fed zero fiber, control, or HAMSAB diet from E0.5 (5 month NOR: WT zero fiber $n = 18$, WT control $n = 19$, WT HAMSAB $n = 22$, AD zero fiber $n = 20$, AD control $n = 22$, AD HAMSAB $n = 23$; 6 month NOR: WT zero fiber $n = 32$, WT control $n = 20$, WT HAMSAB $n = 28$, AD zero fiber $n = 34$, AD control $n = 20$, AD HAMSAB $n = 28$). **f**, Alternation rate of T maze of 6 month WT mice and 5xFAD mice fed zero fiber, control, or HAMSAB diet from E0.5 (WT zero fiber $n = 21$, WT control $n = 18$, WT HAMSAB $n = 26$, AD zero fiber $n = 25$, AD control $n = 20$, AD HAMSAB $n = 31$). **g**, **h**, Recognition index of NOR test of 5 month (**g**) and 6 month (**h**) WT mice and 5xFAD mice fed zero fiber, control, or HAMSAB diet from 1 month (5 month NOR: WT zero fiber $n = 13$, WT control $n = 16$, WT HAMSAB $n = 13$, AD zero fiber $n = 18$, AD control $n = 9$, AD HAMSAB $n = 15$; 6 month NOR: WT zero fiber $n = 13$, WT control $n = 14$, WT HAMSAB $n = 16$, AD zero fiber $n = 17$, AD control $n = 9$, AD HAMSAB $n = 18$). **i**, Alternation rate of T maze of 6 month WT mice and 5xFAD mice fed zero fiber, control, or HAMSAB diet from 1 month (WT zero fiber $n = 7$, WT control $n = 16$, WT HAMSAB $n = 12$, AD zero fiber $n = 19$, AD control $n = 9$, AD HAMSAB $n = 13$). **j**, **k**, Recognition index of NOR test of 5 month (**j**) and 6 month (**k**) WT mice and 5xFAD mice whose mothers were fed zero fiber, control, or HAMSAB diet (5 month NOR: WT zero fiber $n = 11$, WT control $n = 19$, WT HAMSAB $n = 19$, AD zero fiber $n = 17$, AD control $n = 22$, AD HAMSAB $n = 15$; 6 month NOR: WT zero fiber $n = 5$, WT control $n = 20$, WT HAMSAB $n = 15$, AD zero fiber

Table 1. Dietary compositions for zero fiber diet, control diet (AIN93G), HAMSAB diet, HAMSA diet, HAMSB diet, and high-fiber diet

	Zero fiber (g/kg)	Control (AIN93G) (g/kg)	HAMSAB (g/kg)	HAMSA (g/kg)	HAMSB (g/kg)	High fiber (g/kg)
Ingredient						
Casein (acid)	200	200	200	200	200	200
Sucrose	0	100	100	100	100	0
Canola oil	70	70	0	0	0	70
Sunflower oil	0	0	70	70	70	0
Cellulose	0	50	50	50	50	50
Wheat starch	0	404	0	0	0	0
Dextrinized starch	0	132	0	0	0	0
Maize starch	0	0	236	386	386	0
L-methionine	3.0	3.0	3.0	3.0	3.0	3.0
Calcium carbonate	13.1	13.1	13.1	13.1	13.1	13.1
Sodium chloride	2.6	2.6	2.6	2.6	2.6	2.6
AIN93 trace minerals	1.4	1.4	1.4	1.4	1.4	1.4
Potassium citrate	2.5	2.5	2.5	2.5	2.5	2.5
Potassium dihydrogen phosphate	6.9	6.9	6.9	6.9	6.9	6.9
Potassium sulphate	1.6	1.6	1.6	1.6	1.6	1.6
Choline chloride (75%)	2.5	2.5	2.5	2.5	2.5	2.5
AIN93 vitamins	10	10	10	10	10	10
Dextrose monohydrate	686	0	0	0	0	0
HAMSA	0	0	150	150	0	0
HAMSB	0	0	150	0	150	0
Gel crisp starch	0	0	0	0	0	636
Calculated nutritional parameters as fed						
Protein	19.40%	19.40%	19.40%	19.40%	19.40%	19.40%
Total fat	7%	7%	7%	7%	7%	7%
Crude fiber	0%	4.70%	7.10%	5.80%	5.80%	9.70%
AD fiber	0%	4.70%	5.80%	5.80%	5.80%	9.70%
Digestible energy	16.9 MJ/kg	16.1 MJ/kg	16.3 MJ/kg	16.3 MJ/kg	16.3 MJ/kg	15.6 MJ/kg
% total calculated digestible energy from lipids	16%	16%	16%	16%	16%	16.40%
% total calculated digestible energy from protein	21%	21%	21%	21%	21%	21.90%

Bifidobacterium, *Bacteroides*, and *Clostridium* (Extended Data Fig. 2-2f). Thus, the three diets had profound effects on bacterial ecology in the gut. We also examined the role of SCFAs in gut physiology which were analyzed with two-way ANOVA and Tukey's multiple comparison test. Interestingly, 5xFAD mice fed a zero fiber diet had 114.2% larger fibrotic areas ($p = 2 \times 10^{-4}$, Extended Data Fig. 2-2e,g, genotype effect: $F_{(1,59)} = 4.77$ $p = 3.2 \times 10^{-2}$, diet effect: $F_{(2,59)} = 10.17$, $p = 2 \times 10^{-4}$, interaction: $F_{(2,59)} = 1.42$, $p = 0.24$), 48.6% less mucin-producing goblet cells (Extended Data Fig. 2-2f,h, $p = 1 \times 10^{-4}$, genotype effect: $F_{(1,31)} = 1.87$ $p = 0.18$, diet effect: $F_{(2,31)} = 23.03$, $p < 1 \times 10^{-4}$, interaction: $F_{(2,31)} = 0.019$, $p = 0.98$), 21.6% shorter villi (Extended Data Fig. 2-2i, $p = 0.0145$, genotype effect: $F_{(1,37)} = 5.86$ $p = 2 \times 10^{-2}$, diet effect: $F_{(2,37)} = 7.31$, $p = 2 \times 10^{-3}$, interaction: $F_{(2,37)} = 0.7$, $p = 0.5$), and 70.6% lower large intestine weights (Extended Data Fig. 2-2j, $p < 1 \times 10^{-10}$, genotype effect: $F_{(1,54)} = 3.01$ $p = 8.8 \times 10^{-2}$, diet effect: $F_{(2,54)} = 134$, $p < 1 \times 10^{-6}$, interaction: $F_{(2,54)} = 0.2$, $p = 0.81$) compared with 5xFAD mice fed

HAMSAB diet. Also, the number of goblet cells and large intestine weight are altered by diets in WT mice (Extended Data Fig. 2-2h,j). These suggest that SCFAs reduce chronic intestinal inflammation, promote mucin production, and alter gut morphology in both 5xFAD and WT mice. Together, these data show that fiber/SCFAs play a key role in gut microbiome composition and gut physiology.

At 5 months, diet ($F_{(2118)} = 19.94$, $p < 1 \times 10^{-6}$) and genotype ($F_{(2118)} = 13.14$, $p = 7 \times 10^{-6}$) had a significant effect on cognition (Fig. 2d), and their interaction is also significant ($F_{(2118)} = 21.74$, $p = 8 \times 10^{-6}$). We did not detect a deficit in cognition in 5xFAD mice fed control diet and HAMSAB diet compared with their WT littermates, nor did the diet significantly influence the recognition memory of WT mice (Fig. 2d). In contrast, 5xFAD mice fed zero fiber diet had a 32.2% lower recognition index at 5 months compared with 5xFAD mice fed control diet (Fig. 2d, $p = 1.57 \times 10^{-5}$). Similar results were observed at 3.5 months (Extended Data Fig. 2-3a). Together, these findings demonstrate that lack of fiber accelerates cognitive decline in 5xFAD mice.

At 6 months, diet ($F_{(2,156)} = 21.71$, $p < 1 \times 10^{-6}$) and genotype ($F_{(1,156)} = 24.6$, $p = 1.8 \times 10^{-6}$) had a significant effect on cognition (Fig. 2e), and their interaction is also significant ($F_{(2,156)} = 15.72$, $p < 1 \times 10^{-6}$). We detected a 21.8% lower recognition index in 5xFAD mice fed a control diet compared with their WT littermates (Fig. 2e, $p = 6.02 \times 10^{-4}$). Furthermore, the recognition index of 5xFAD mice fed HAMSAB diet was 38% higher than 5xFAD mice fed control diet (Fig. 2e, $p < 1 \times 10^{-6}$). We observed similar results in 5xFAD mice fed a high-fiber diet (high resistant starch) (Extended Data Fig. 2-3b), which was previously shown to protect against cardiovascular disease (Marques et al., 2017). To confirm these results, we utilized an

←

$n = 17$, AD control $n = 20$, AD HAMSAB $n = 16$). *I*, Alternation rate of T maze of 6 month WT mice and 5xFAD mice whose mothers were fed with zero fiber, control, or HAMSAB diet (WT zero fiber $n = 13$, WT control $n = 18$, WT HAMSAB $n = 9$, AD zero fiber $n = 16$, AD control $n = 20$, AD HAMSAB $n = 15$). *m*, *n*, Recognition index of NOR test (*m*) and alternation rate of T maze test (*n*) of 6 month *Gpr41/43/109a*$^{+/+}$, *Gpr41/43/109a*$^{-/-}$, *Gpr41/43*$^{-/-}$, WT/5xFAD mice fed HAMSAB diet from 1 month (NOR: WT *Gpr41/43/109a*$^{+/+}$ $n = 16$, WT *Gpr41/43/109a*$^{-/-}$ $n = 8$, WT *Gpr41/43*$^{-/-}$ $n = 8$, AD *Gpr41/43/109a*$^{+/+}$ $n = 18$, AD *Gpr41/43/109a*$^{-/-}$ $n = 7$, AD *Gpr41/43*$^{-/-}$ $n = 7$; T maze: WT *Gpr41/43/109a*$^{+/+}$ $n = 12$, WT *Gpr41/43/109a*$^{-/-}$ $n = 8$, WT *Gpr41/43*$^{-/-}$ $n = 8$, AD *Gpr41/43/109a*$^{+/+}$ $n = 13$, AD *Gpr41/43/109a*$^{-/-}$ $n = 8$, AD *Gpr41/43*$^{-/-}$ $n = 7$). Data are mean ± SEM. *$p < 0.05$; **$p < 0.01$; ***$p < 0.001$; ****$p < 0.0001$; two-way ANOVA and Tukey's multiple comparison test. Extended Data Figures 2-1, 2-2, and 2-3 support Figure 2.

alternative cognition assay, the spontaneous T maze alternation test, and similar results were observed (Fig. 2f). At 8 months, 5xFAD mice fed HAMSAB diet showed 28.6% higher recognition memory in NOR ($p = 1.2 \times 10^{-3}$, diet ($F_{(2,90)} = 24.43$, $p < 1 \times 10^{-6}$) and genotype ($F_{(1,90)} = 22.1$, $p = 9.2 \times 10^{-6}$) but no improvement in T maze compared with 5xFAD mice fed control diet (Extended Data Fig. 2-3c,d). Notably, we detected a 19.7% decline in recognition memory for WT mice fed zero fiber diet compared with WT mice fed control diet (Extended Data Fig. 2-3c, $p = 3.7 \times 10^{-3}$), suggesting that SCFAs may generally benefit cognition and memory, and not only in the context of disease. In summary, these data show that SCFA supplementation improves recognition memory at 6 months.

As HAMSAB diet releases high levels of both acetate and butyrate, we investigated whether the protective effect could be replicated by acetate or butyrate alone, supplied by HAMSA or HAMSB diets, respectively. Similar to 5xFAD mice fed a HAMSAB diet, mice fed HAMSB alone showed a 32% higher recognition index compared with 5xFAD mice fed control diet (Extended Data Fig. 2-3e, $p = 7.5 \times 10^{-4}$), suggesting that butyrate alone protects against AD cognitive decline at 6 months. HAMSA 5xFAD mice showed 34.5% higher recognition index compared with the zero fiber 5xFAD mice (Extended Data Fig. 2-3e, $p = 3.6 \times 10^{-4}$); however, the difference between HAMSA 5xFAD mice and control 5xFAD mice was not significant (Extended Data Fig. 2-3e, $p = 0.1$), indicating that, although acetate plays a beneficial role in cognition, the protective effect of acetate is weaker than butyrate.

To unveil whether the effect of SCFAs could be achieved after weaning, we fed another cohort of mice with the different diets starting from 1 month of age. Surprisingly, there was no difference between 5xFAD mice fed different diets in NOR at 5 months (Fig. 2g), suggesting that a zero fiber diet does not accelerate cognitive decline when administered from 1 month of age. Nonetheless, 5xFAD mice fed HAMSAB diet exhibited 39.6% higher scores ($p = 3.1 \times 10^{-3}$) in NOR (Fig. 2h, genotype effect: $F_{(1,81)} = 18.69$, $p = 4.3 \times 10^{-5}$, diet effect: $F_{(2,81)} = 10.65$, $p = 7.8 \times 10^{-5}$, interaction is not significant) and 41.5% higher score ($p = 0.0016$) in T maze (Fig. 2i, genotype effect: $F_{(1,70)} = 19.72$ $p = 3.2 \times 10^{-5}$, diet effect: $F_{(2,70)} = 8.144$, $p = 6.6 \times 10^{-4}$, interaction: $F_{(2,70)} = 3.844$, $p = 0.026$) test compared with the control 5xFAD mice at 6 months, showing that fiber/SCFA supplementation from 1 month exerted protective effects on recognition and spatial working memory.

The above findings suggested that *in utero* or early life nutrition of the mother may contribute to AD in the offspring. The "developmental origin of disease" concept assumes that experiences *in utero* or early life influence disease later in life. Recently, we showed that asthma is highly influenced by fiber intake by the mother (Thorburn et al., 2015). To understand how maternal diets affect AD progression, we fed pregnant mice a zero fiber diet, control diet, or HAMSAB diet from E0.5. The pups were all fed a control diet after weaning. At 5 months, 5xFAD mice whose mothers were fed zero fiber diet showed accelerated cognitive decline in NOR compared with other AD groups (Fig. 2j, genotype effect: $F_{(1,97)} = 7.9$ $p = 5.8 \times 10^{-3}$, diet effect: $F_{(2,97)} = 7.028$, $p = 1.4 \times 10^{-3}$, interaction: $F_{(2,97)} = 5.374$, $p = 6.1 \times 10^{-3}$). Feeding mothers HAMSAB improved 5xFAD offspring memory in T maze (Fig. 2l, genotype effect: $F_{(1,85)} = 26.52$ $p = 1.6 \times 10^{-6}$, diet effect: $F_{(2,85)} = 6.73$, $p = 1.9 \times 10^{-3}$, interaction: $F_{(2,85)} = 2.375$, $p = 0.099$) but not in NOR (Fig. 2k, genotype effect: $F_{(1,87)} = 29.9$ $p < 1 \times 10^{-6}$, diet effect: $F_{(2,87)} = 1.176$, $p = 0.3$, interaction: $F_{(2,87)} = 0.06$, $p = 0.93$) at 6 months.

Together, these data suggest that SCFA supplementation during pregnancy and/or lactation plays an important role in offspring cognition and AD progression.

Finally, to test whether the protective effect of HAMSAB on cognition was mediated by GPCRs, we fed triple and double GPCR KO mice a HAMSAB diet from 1 month of age. The memory impairment induced by deletion of *Gpr41* and *Gpr43* or all three receptors in WT and 5xFAD mice at 6 months was not rescued by the HAMSAB diet (Fig. 2m,n, genotype effect: $F_{(1,58)} = 0.44$ $p = 0.51$, diet effect: $F_{(2,58)} = 36.34$, $p < 1 \times 10^{-6}$, interaction: $F_{(2,58)} = 1.53$, $p = 0.22$), suggesting a predominant role of metabolite-sensing GPCRs in the mechanism mediating SCFA protection against cognitive decline.

Dietary fiber alters microglial morphology and induces AHN
To understand how SCFAs affect brain pathology, we investigated microglia and Aβ load. 5xFAD mice have more microglia than WT mice (Extended Data Fig. 3-1a-d); however, we did not observe differences in hippocampal and cortical microglial density between diets [Extended Data Fig. 3-1a-d, two-way ANOVA and Tukey's multiple comparison test, genotype effect (DG): $F_{(1,47)} = 43.5$ $p < 1 \times 10^{-6}$, diet effect (DG): $F_{(2,47)} = 0.42$, $p = 0.65$, interaction (DG): $F_{(2,47)} = 0.52$, $p = 0.59$; genotype effect (CX): $F_{(1,47)} = 55.65$ $p < 1 \times 10^{-6}$, diet effect (CX): $F_{(2,47)} = 0.5$, $p = 0.6$, interaction (CX): $F_{(2,47)} = 0.48$, $p = 0.62$]. In WT brains, mice fed a zero fiber diet had microglia, which were less ramified, with 44.3% shorter processes ($p = 9.9 \times 10^{-3}$), 45.7% less branch points ($p = 4.3 \times 10^{-2}$), and 20.9% larger cell bodies ($p = 6.4 \times 10^{-3}$) compared with those from mice fed the HAMSAB diet [Fig. 3a-d, one-way ANOVA and Tukey's multiple comparison test, diet effect (process length): $F_{(2,21)} = 0.78$, $p = 5.3 \times 10^{-3}$; diet effect (branch point): $F_{(2,21)} = 4.897$, $p = 1.8 \times 10^{-2}$; diet effect (cell body diameter): $F_{(2,21)} = 7.835$, $p = 2.9 \times 10^{-3}$], suggesting that lack of fiber induced activated microglial morphology in WT mice. No morphologic differences were observed in plaque distal microglia from 5xFAD mice fed different diets, and we were unable to quantify the morphology of plaque associated microglia because of the clustering phenotype [Extended Data Fig. 3-1e-h, one-way ANOVA and Tukey's multiple comparison test, diet effect (process length): $F_{(2,26)} = 0.4406$, $p = 0.65$; diet effect (branch point): $F_{(2,26)} = 0.3203$, $p = 0.728$; diet effect (cell body diameter): $F_{(2,26)} = 1.122$, $p = 0.341$]. However, in 5xFAD mice, we observed a 41% increase in the number of microglia clustering within 20 μm of a plaque in the hippocampus of mice fed HAMSAB diet compared with mice fed a zero fiber diet [Fig. 3e,f, $p = 0.019$, one-way ANOVA and Tukey's multiple comparison test, diet effect (branch point): $F_{(2,26)} = 4.536$, $p = 0.024$) despite the volume of Aβ plaques phagocytosed by microglia being similar between diets (Extended Data Fig. 3-1i, one-way ANOVA and Tukey's multiple comparison test, diet effect (branch point): $F_{(2,26)} = 1.139$, $p = 0.33$]. Nevertheless, 5xFAD mice fed HAMSAB diet had 20.4% smaller plaques ($p = 6.7 \times 10^{-2}$) and 34.9% less plaque covered area ($p = 8.2 \times 10^{-2}$) in the cortex compared with 5xFAD mice fed a zero fiber diet. The Aβ load in the DG was similar between diets (Fig. 3g,h; Extended Data Fig. 3-1j, plaque number genotype effect: $F_{(1,52)} = 14.01$ $p = 4 \times 10^{-3}$, diet effect: $F_{(2,52)} = 2.44$, $p = 9.6 \times 10^{-2}$, interaction: $F_{(2,52)} = 0.247$, $p = 0.78$) Together, these data suggest that SCFAs influence microglial morphology and clustering, and may reduce Aβ pathology at 6 months.

Finally, to examine whether SCFAs play a role in AHN, we quantified the number of DCX+ neurons in the DG (Fig. 3i, two-way ANOVA and Tukey's multiple comparison test,
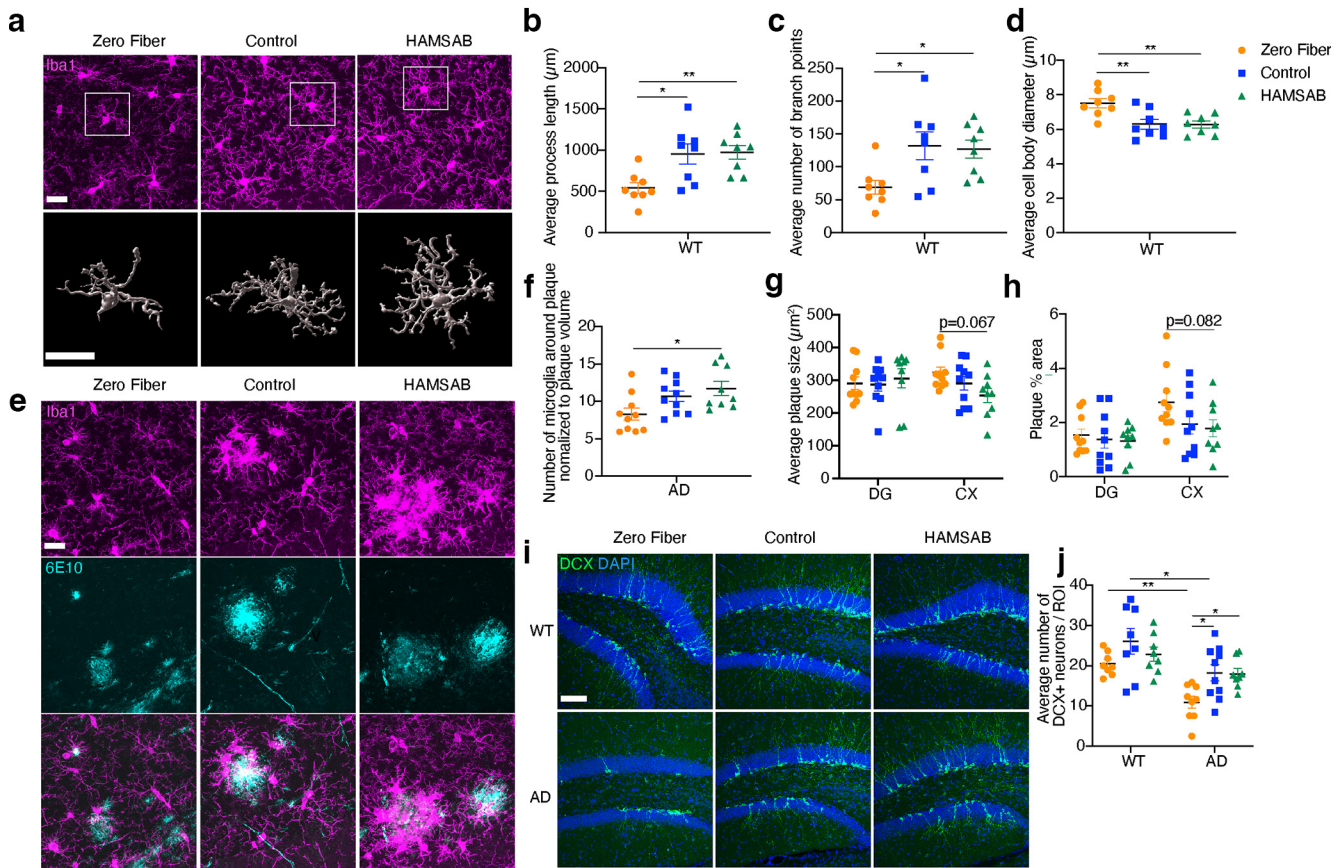
Figure 3. Dietary fiber influences microglia, Aβ pathology, and neurogenesis. *a*, Representative immunofluorescence images and Imaris 3D reconstruction of Iba1$^+$ microglia (magenta) from the DG of 6 month WT mice fed zero fiber, control, or HAMSAB diet. Scale bar, 20 μm. *b–d*, Imaris-based automatic quantification of microglial morphology ($n = 8$). *e*, Representative immunofluorescence images of Iba1$^+$ microglia (magenta) and 6E10$^+$ plaques (cyan) from the DG of 6 month 5xFAD mice fed zero fiber, control, or HAMSAB diet. Scale bar, 20 μm. *f*, Average number of microglia surrounding 20 μm radius of a plaque in DG, normalized to plaque volume (AD zero fiber $n = 10$, AD control $n = 10$, AD HAMSAB $n = 9$). *g, h*, Average plaque size (*g*) and the percentage of 6E10$^+$ area (*h*) in DG and cortex of 6-month-old 5xFAD mice fed zero fiber, control, or HAMSAB diet (AD zero fiber $n = 10$, AD control $n = 10$, AD HAMSAB $n = 9$). *i, j*, Representative immunofluorescence images (*i*) and quantification (*j*) of DCX$^+$ newly born neurons (green) from the DG of 6 month 5xFAD mice fed zero fiber, control, or HAMSAB diet. Scale bar, 100 μm. WT zero fiber $n = 8$, WT control $n = 8$, WT HAMSAB $n = 8$, AD zero fiber $n = 10$, AD control $n = 10$, AD HAMSAB $n = 9$. Data are mean ± SEM. *$p < 0.05$; **$p < 0.01$; two-way ANOVA (*g,h,j*) or one-way ANOVA (*b–d,f*) and Tukey's multiple comparison test. Extended Data Figure 3-1 supports Figure 3.

genotype effect: $F_{(1,45)} = 22.39$ $p < 1 \times 10^{-3}$, diet effect: $F_{(2,45)} = 6.193$, $p = 4.2 \times 10^{-3}$, interaction: $F_{(2,45)} = 0.72$, $p = 0.49$). 5xFAD mice fed a control diet had 30.3% less DCX$^+$ neurons compared with their WT littermates (Fig. 3j, $p = 1.5 \times 10^{-2}$). In 5xFAD mice, a 40.1% reduction in DCX$^+$ neurons was noted in mice that received a zero fiber diet compared with the control diet group (Fig. 3j, $p = 1.7 \times 10^{-2}$), showing that lack of fiber impairs AHN in 5xFAD mice.

Dietary fiber alters microglial transcriptome at an early stage
To shed light into the molecular events underpinning the changes in microglia observed as a consequence of the different diets, we fed pregnant mothers the diets from E0.5, and performed bulk RNA sequencing (RNA-seq) in isolated microglia from 3-week-old pups (Fig. 4a; Extended Data Fig. 4-1a). Microglia displayed distinct gene expression profiles as shown in the multidimensional scaling plot (Fig. 4b). In the first dimension, HAMSAB microglia were separated from control and zero fiber microglia. Genotype was not a significant covariate in this model; therefore, we pooled microglia from WT and 5xFAD mice fed the same diet for subsequent analyses. We modeled diet as a continuous factor. Overall, we identified 113 fiber-related DEGs; of these, 72 DEGs were positively correlated with the amount of fiber, and 41 DEGs correlated inversely with the

amount of fiber (Fig. 4c). Gene ontology analysis revealed that SCFAs significantly upregulated genes related to multiple immune pathways (Fig. 4d). For example, nonclassical MHC Class Ib genes involved in antigen presentation were significantly upregulated by fiber, such as *B2m*, *H2-D1*, *H2-Q7*, *H2-M3*, *H2-K1*, and *H2-Q6* (Fig. 4e). In addition, fiber upregulated the expression of genes involved in T-cell activation, including *Cd83*, *Ctsl*, *Il2rg*, *Rsad2*, and *Cd274* (Fig. 4f). Interestingly, genes involved in the IFNβ response, such as *Ifit1*, *Ifit3*, *Ifitm3*, and *Lgtp*, were also regulated by fiber (Fig. 4g). Furthermore, SCFA supplementation upregulated genes contributing to macrophage migration, such as *Cd9*, *Ccl5*, *Thbs1*, *Slamf8*, and *Csf1* (Fig. 4h). In contrast, fiber downregulated genes related to cell development, such as positive regulation of Notch signaling pathway and myeloid cell development (Fig. 4d). Next, we examined the expression of core genes in DAM, a protective microglia type in AD (Keren-Shaul et al., 2017). ROAST analysis revealed that 69.9% DAM marker genes were upregulated by fiber (Fig. 4i), indicating that fiber significantly enriched the DAM transcriptomic signature ($p = 7.5 \times 10^{-4}$). These data show that dietary fiber can alter the microglial transcriptome, which might explain the microglial clustering phenotype and cognitive changes observed at later stages in mice fed a HAMSAB diet.
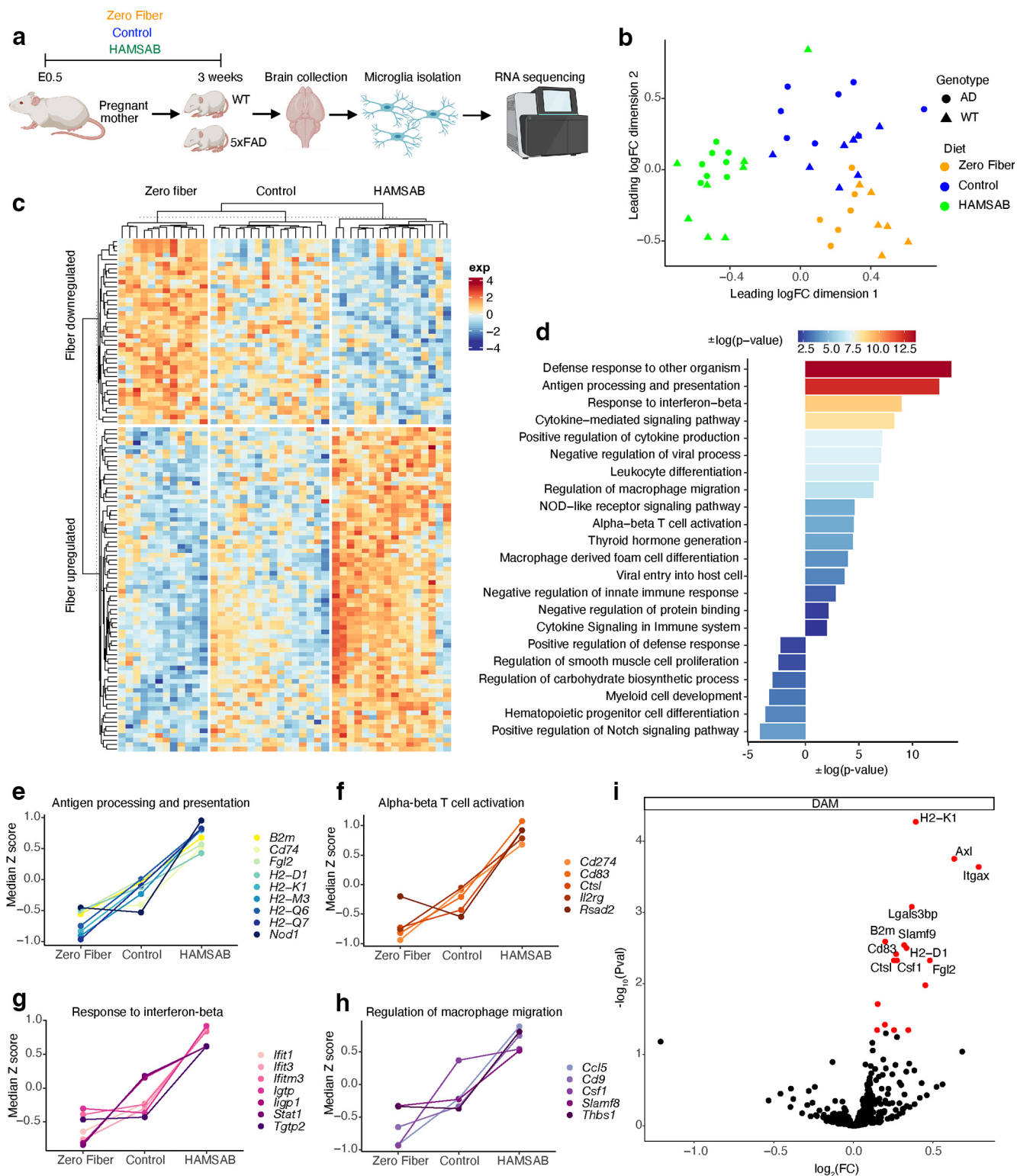
Figure 4. Maternal dietary fiber intake alters the microglial transcriptome at 3 weeks. ***a***, Schematic of experimental design created with Biorender.com. WT zero fiber $n = 6$, WT control $n = 8$, WT HAMSAB $n = 8$, AD zero fiber $n = 6$, AD control $n = 8$, AD HAMSAB $n = 8$. ***b***, Multidimensional scaling of gene expression profiles of microglia isolated from 3 week WT and 5xFAD mice whose mothers were fed zero fiber, control, or HAMSAB diet. ***c***, Hierarchical clustering of microglial transcriptomes. ***d***, Gene Ontology analysis shows fiber-upregulated and fiber-downregulated pathways. ***e–h***, Representative fiber-upregulated gene clusters. ***i***, Volcano plot of DAM core gene expression. Red dots indicate fiber-upregulated DEGs. Positive $\log_2 FC$ indicates that gene expression is positively associated with fiber. Negative $\log_2 FC$ indicates that gene expression is negatively associated with fiber. Extended Data Figure 4-1 supports Figure 4.

Fiber/SCFAs alter T-cell profiles in the brain

Peripheral immune cell infiltration contributes to AD progression (Dionisio-Santos et al., 2019). CD8^{+} T-cell infiltration has been observed in the elderly and in AD patients, as well as in aged and AD mouse models (Ferretti et al., 2016; Laurent et al., 2017; Dulken et al., 2019; Gate et al., 2020). Furthermore, the influence of SCFAs on T cells is well documented (Furusawa et al., 2013; Bachem et al., 2019). T cells were examined in our

experimental model via flow cytometric analyses of the brains of 6 month WT mice and 5xFAD mice fed zero fiber, control, and high-fiber diets (Fig. 5a). Using intravenous labeling with a fluorescently conjugated anti-CD45 antibody, we were able to distinguish leukocytes localized within the brain parenchyma from those in circulation. Data were analyzed with two-way ANOVA followed by Tukey's multiple comparison test. Fiber significantly altered T-cell numbers in the brain. We did not detect a difference in $CD4^+$ T cells between WT and 5xFAD mice fed the control diet; however, 5xFAD mice fed the zero fiber diet had significantly more $CD4^+$ T cells compared with their WT littermates (Fig. 5b, $p = 0.0244$, genotype effect: $F_{(1,41)} = 9.78$ $p = 3.2 \times 10^{-3}$, diet effect: $F_{(2,41)} = 4.342$, 1.9×10^{-2}, interaction: $F_{(2,41)} = 0.84$, $p = 0.438$). The number of $CD8^+$ T cells was significantly higher in 5xFAD mice compared with their WT littermates with both the control ($p = 1.8 \times 10^{-3}$) and the zero fiber diets ($p = 5.3 \times 10^{-3}$) (Fig. 5c, genotype effect: $F_{(1,41)} = 34.69$ $p < 1 \times 10^{-6}$, diet effect: $F_{(2,41)} = 2.536$, $p = 9.1 \times 10^{-2}$, interaction: $F_{(2,41)} = 0.21$, $p = 0.81$). Notably, expression of CD69, a marker of early activation and tissue residency (Cibrián and Sánchez-Madrid, 2017), was negatively associated with dietary fiber in 5xFAD mice. 5xFAD mice fed a high-fiber diet had significantly less $CD69^+$ $CD4^+$ T cells (Fig. 5d, $p = 4.4 \times 10^{-3}$, genotype effect: $F_{(1,41)} = 19.23$ $p < 1 \times 10^{-4}$, diet effect: $F_{(2,41)} = 6.07$, $p = 4.9 \times 10^{-3}$, interaction: $F_{(2,41)} = 1.39$, $p = 0.26$) and $CD69^+$ $CD8^+$ T cells (Fig. 5e, $p = 2 \times 10^{-3}$, genotype effect: $F_{(1,42)} = 28.53$ $p < 3.4 \times 10^{-6}$, diet effect: $F_{(2,42)} = 6.189$, $p = 4.4 \times 10^{-3}$, interaction: $F_{(2,42)} = 2.613$, $p = 8.5 \times 10^{-2}$) compared with 5xFAD mice fed the zero fiber diet. Thus, dietary fiber dampens T-cell recruitment and activation into the brain, consistent with the anti-inflammatory nature of SCFAs.

Discussion

Traditionally, two of the major risk factors for AD are age and genetics (Masters et al., 2015). However, some populations have a remarkably low incidence of AD (Lopez and Kuller, 2019), suggesting the existence of overriding environmental factors. In humans, the Mediterranean diet plays a protective role in cognition (Lourida et al., 2013). Gut microbiota composition changes significantly in preclinical and symptomatic AD patients (Vogt et al., 2017; Ferreiro et al., 2023). The most likely mechanism of dietary protection is metabolites produced by the gut microbiota, which could travel to the blood and brain.

In our study, we show that dietary fiber profoundly affects cognitive decline in 5xFAD and WT mice. Metabolite-sensing GPCRs are the major mechanisms by which SCFAs mediate biological effects (Tan et al., 2017). Our study showed increased amyloid load in single, double, and triple GPCR KO mice, suggesting that GPCRs may participate in amyloid clearance, production, or processing. However, the amyloid load was not changed in 6 month 5xFAD mice fed different diets, suggesting that SCFA alone is not sufficient to alter amyloid pathology, or Gpr41 and Gpr43 may play other roles in addition to sensing SCFAs.

Microglia are central to AD pathogenesis (Streit et al., 2021). In our study, zero fiber diet led to activated microglial morphology in WT mice. Notably, we found that HAMSAB diet induced microglial clustering around plaques. Clustering microglia form a barrier via TREM2/DAP12 signaling, thus promoting plaque compaction and reducing axonal dystrophy (Yuan et al., 2016). In addition, disease-associated microglia, usually clustered around plaques, are phagocytic cells responsible for $A\beta$ clearance (Keren-Shaul et al., 2017) with genetic evidence supportive of their

beneficial role in AD (Deczkowska et al., 2018). Another study showed that dietary inulin restored microglia expression of aging-, inflammation-, sensome-related markers and TNF-α secretion in aged mice (Vailati-Riboni et al., 2022). In our study, knocking out GPCRs did not alter microglial phenotype in WT and 5xFAD mice. Indeed, Gpr43 and Gpr41 are not expressed by microglia in mouse brain (Caetano-Silva et al., 2023). Thus, other mechanisms are involved in SCFA–microglia interaction. A study showed that SCFAs inhibited the inflammatory response of LPS-induced microglia via HDAC inhibition (Caetano-Silva et al., 2023), suggesting that SCFAs may impact epigenetic regulation in microglia. An alternative explanation might be that peripheral cells expressing Gpr41 and Gpr43 transduce a cytokine signal that affects the brain; therefore, more studies are needed to investigate the cytokine profiles in the periphery and the CNS.

We showed that reduced fiber intake impaired AHN in 5xFAD mice but not WT mice at 6 months. Supplementation of sodium butyrate or transplantation of butyrate-producing bacteria has been reported to increase AHN in mouse hippocampus (Kim et al., 2009; Kundu et al., 2019). Increasing AHN improved long-term memory and rescued cognitive deficit in aged mice (McAvoy et al., 2016; Meyers et al., 2016). Triple depletion of Gpr41, Gpr43, and Gpr109a led to impaired AHN in both 5xFAD and WT mice at 6 months, while double KO of Gpr41 and Gpr43 did not affect AHN, although their cognitive function is impaired at 6 months. One study showed that inducing AHN alone was not sufficient to improve memory in 5xFAD mice (Choi et al., 2018), suggesting that other pathways are involved in SCFA/GPCR-related cognitive changes. For example, sodium butyrate treatment improved synapse plasticity with more abundant dendritic spines in 5xFAD mice (Jiang et al., 2021), which could be another possible mechanism.

It is possible that SCFAs are transported to the brain, where they influence brain cell functions. Our findings suggest that SCFAs cross the blood–brain barrier and insufficient intake of fiber may adversely affect SCFA entry to the brain. SCFA concentrations in the brain were higher than in peripheral blood. This could be explained by the active transport of SCFAs into the brain, as indicated previously (Frost et al., 2014), and is consistent with the expression of the SCFA transporter monocarboxylate transporter 1 on brain endothelium (Vijay and Morris, 2014; Kurosawa et al., 2018). WT mice and 5xFAD mice fed HAMSAB diet showed similar levels of butyrate and acetate in the brain; however, their cognitive and pathologic phenotype is different, suggesting that SCFA-mediated effects are genotype-dependent. 5xFAD mice may be more sensitive to SCFAs in the brain as they display amyloid deposition, gliosis, leukocyte infiltration, and neurodegeneration (Oakley et al., 2006); these features may lead to different sensitivity to SCFAs. We are unsure whether SCFAs levels will change with age as we only measured brain SCFA levels at 6 months. In addition to interacting directly with brain cells, SCFAs may also exert their effects indirectly through vagus nerve signaling. Vagus nerve signaling is essential for mediating satiety, stress, and mood (Goehler et al., 2005; Forsythe et al., 2014; Browning et al., 2017). Previous study shows that gut vagal sensory signaling regulates hippocampus-dependent episodic and spatial memory via multiorder brainstem-septal pathway (Suarez et al., 2018). Additionally, GPR41 expressed in vagal neurons regulates feeding behavior and mediates propionate-induced food intake decrease (Cook et al., 2021). Therefore, further investigation may focus on vagus nerve signaling in mice supplemented with dietary fiber.
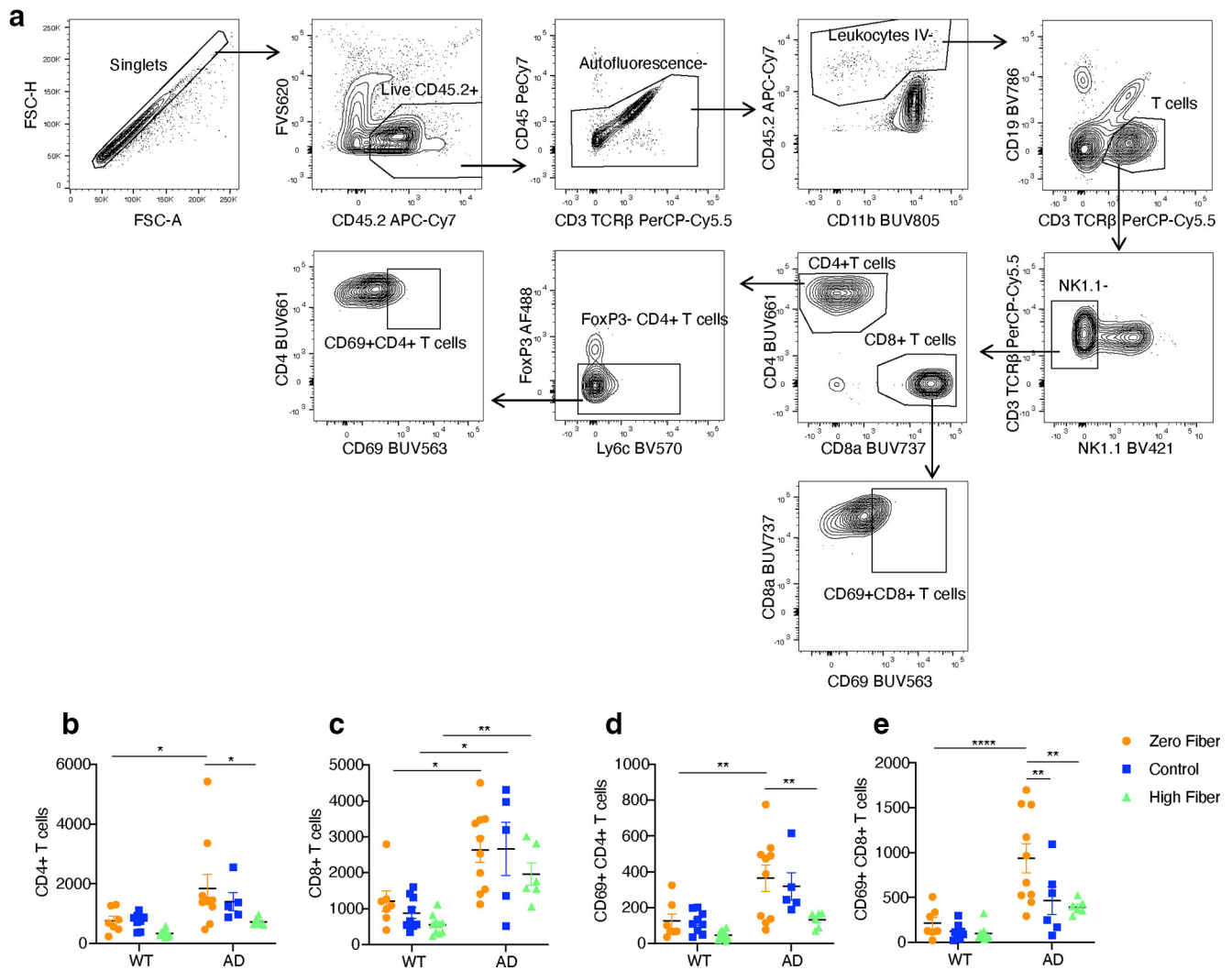
Figure 5. Dietary fiber affects brain T-cell signature. *a*, A gating strategy used to identify populations of immune cells. *b–e*, Quantification of the number of CD4$^+$ T cells (*b*), CD8$^+$ T cells (*c*), CD69$^+$ CD4$^+$ T cells (*d*), and CD69$^+$ CD8$^+$ T cells (*e*) from 6 month WT mice and 5xFAD mice fed zero fiber, control, or high-fiber diet (WT zero fiber $n = 7$, WT control $n = 9$, WT HAMSAB $n = 10$, AD zero fiber $n = 10$, AD control $n = 5$, AD HAMSAB $n = 6$). Data are mean ± SEM. *$p < 0.05$; **$p < 0.01$; ***$p < 0.001$; ****$p < 0.0001$; two-way ANOVA and Tukey's multiple comparison test.

Maternal dietary patterns have been closely linked with offspring's development and health. Our study shows that maternal dietary fiber intake is critical in offspring's cognition in 5xFAD mice, suggesting that disease prevention may be achieved by a healthy diet during mother's pregnancy or lactation. We did not observe a behavioral difference in WT mice; however, a recent study showed that maternal low-fiber diet induced cognitive deficit and impaired synaptic plasticity in the offspring of C57BL/6J mice, and butyrate reversed the adverse effect through HDAC4 signaling (Yu et al., 2020), suggesting that maternal fiber is critical for cognition under neurologically healthy conditions.

Maternal SCFAs were able to enter offspring's' circulation during early development (Thorburn et al., 2014; Kimura et al., 2020). For instance, maternal high-fiber diet led to higher levels of plasma SCFAs in the offspring at E18.5 compared with maternal low-fiber group (Kimura et al., 2020). More importantly, metabolite-sensing GPCRs were already expressed in multiple tissues at the embryonic stage, such as sympathetic nerves, pancreas, and intestinal epithelium (Kimura et al., 2020). Moreover, maternal SCFAs protected against asthma in the offspring by affecting fetal lung transcriptome (Thorburn et al., 2015). It is also possible that SCFA transfer to the offspring via breast milk.

Human breast milk contains SCFAs, although the concentrations vary between studies (20-400 μM for acetate, 100-150 μM for butyrate) (Smilowitz et al., 2013; Stinson et al., 2020), which may be because of differences in maternal lifestyle, sample collection, or analyzing methods.

Our study showed that maternal SCFA intake significantly altered microglial transcriptome in the offspring at 3 weeks. SCFAs dramatically upregulated genes involved in defense response, such as *B2m*, *Fgl2*, and *H2-K1*. Indeed, microglia act as the first line of immune defense and mediate innate and adaptive immune activation during diseases and injury (Bachiller et al., 2018). Maternal SCFAs also significantly upregulated antigen processing and presentation pathways in microglia. Under physiological state, microglia did not present antigens; however, under disease states, microglia present antigen to naive CD4 T cells and cross-present antigen to CD8$^+$ T cells (Jarry et al., 2013; Dando et al., 2019; Moseman et al., 2020), suggesting that microglia are effective antigen-presenting cells during disease and SCFAs may potentially enhance the antigen-presenting ability of microglia. Our results highlight that microglia-T cell interactions may be a potential target in AD. Recently, CD8$^+$ T-cell infiltration was observed in elderly humans, AD patients, as well as in aged and AD mouse models (Ferretti et al.,

2016; Laurent et al., 2017; Dulken et al., 2019; Gate et al., 2020), suggesting that T cells may be involved in aging and AD pathology. Interestingly, $CD4^+$ T cells were present in healthy mouse and human brains, which contribute to microglial maturation and synaptic pruning (Pasciuto et al., 2020). Therefore, T cells in the CNS may be key players during homeostasis and pathologic conditions.

AD joins a growing list of Western lifestyle diseases that involve metabolite-sensing GPCRs and are preventable with dietary fiber/SCFAs in mice (Maslowski et al., 2009; Trompette et al., 2014; Thorburn et al., 2015; Tan et al., 2016; Mariño et al., 2017a; Marques et al., 2017; Kaye et al., 2020; Li et al., 2020). The anti-inflammatory effect of SCFA signaling through metabolite-sensing GPCRs is beneficial in all these conditions, suggesting commonalities in disease etiology or pathogenesis of these Western diseases. HAMSAB is hypothesized to work at many levels: GPCR signaling, HDAC inhibition, beneficial changes to the gut microbiota, improvement of gut integrity and homeostasis, anti-inflammatory effects on cytokines and chemokines, and effects on microglia and other leukocytes. Human AD progresses over decades; thus, there is the potential to intervene early with diets rich in SCFAs to prevent ongoing cognitive decline. Moreover, if a major impact of fiber/SCFAs is during development, there is impetus for mothers-to-be to eat high-fiber diets during pregnancy and breastfeeding.

References

Bachem A, et al. (2019) Microbiota-derived short-chain fatty acids promote the memory potential of antigen-activated $CD8^+$ T cells. Immunity 51:285–297.e5.

Bachiller S, Jiménez-Ferrer I, Paulus A, Yang Y, Swanberg M, Deierborg T, Boza-Serrano A (2018) Microglia in neurological diseases: a road map to brain-disease dependent-inflammatory response. Front Cell Neurosci 12:488.

Ballarini T, et al., DELCODE Study Group (2021) Mediterranean diet, Alzheimer disease biomarkers and brain atrophy in old age. Neurology 96:e2920.

Berti V, et al. (2018) Mediterranean diet and 3-year Alzheimer brain biomarker changes in middle-aged adults. Neurology 90:e1789.

Blacher E, et al. (2019) Potential roles of gut microbiome and metabolites in modulating ALS in mice. Nature 572:474–480.

Bolyen E, et al. (2019) Reproducible, interactive, scalable and extensible microbiome data science using QIIME 2. Nat Biotechnol 37:852–857.

Browning KN, Verheijden S, Boeckxstaens GE (2017) The vagus nerve in appetite regulation, mood, and intestinal inflammation. Gastroenterology 152:730–744.

Caetano-Silva ME, Rund L, Hutchinson NT, Woods JA, Steelman AJ, Johnson RW (2023) Inhibition of inflammatory microglia by dietary fiber and short-chain fatty acids. Sci Rep 13:2819.

Callahan BJ, McMurdie PJ, Rosen MJ, Han AW, Johnson AJ, Holmes SP (2016) DADA2: high-resolution sample inference from Illumina amplicon data. Nat Methods 13:581–583.

Choi SH, et al. (2018) Combined adult neurogenesis and BDNF mimic exercise effects on cognition in an Alzheimer's mouse model. Science 361: eaan8821.

Cibrián D, Sánchez-Madrid F (2017) CD69: from activation marker to metabolic gatekeeper. Eur J Immunol 47:946–953.

Cook TM, Gavini CK, Jesse J, Aubert G, Gornick E, Bonomo R, Gautron L, Layden BT, Mansuy-Aubert V (2021) Vagal neuron expression of the microbiota-derived metabolite receptor, free fatty acid receptor (FFAR3), is necessary for normal feeding behavior. Mol Metab 54:101350.

Costa V, Lugert S, Jagasia R (2015) Role of adult hippocampal neurogenesis in cognition in physiology and disease: pharmacological targets and biomarkers. Handb Exp Pharmacol 228:99–155.

Dando SJ, Kazanis R, Chinnery HR, McMenamin PG (2019) Regional and functional heterogeneity of antigen presenting cells in the mouse brain and meninges. Glia 67:935–949.

Davis C, Bryan J, Hodgson J, Murphy K (2015) Definition of the Mediterranean diet: a literature review. Nutrients 7:9139–9153.

Deacon RM (2006) Housing, husbandry and handling of rodents for behavioral experiments. Nat Protoc 1:936–946.

Deacon RM, Rawlins JN (2006) T-maze alternation in the rodent. Nat Protoc 1:7–12.

Deacon RM, Bannerman DM, Kirby BP, Croucher A, Rawlins JN (2002) Effects of cytotoxic hippocampal lesions in mice on a cognitive test battery. Behav Brain Res 133:57–68.

Deczkowska A, Keren-Shaul H, Weiner A, Colonna M, Schwartz M, Amit I (2018) Disease-associated microglia: a universal immune sensor of neurodegeneration. Cell 173:1073–1081.

DeSantis TZ, Hugenholtz P, Larsen N, Rojas M, Brodie EL, Keller K, Huber T, Dalevi D, Hu P, Andersen GL (2006) Greengenes, a chimera-checked 16S RRNA gene database and workbench compatible with ARB. Appl Environ Microbiol 72:5069–5072.

Dionisio-Santos DA, Olschowka JA, O'Banion MK (2019) Exploiting microglial and peripheral immune cell crosstalk to treat Alzheimer's disease. J Neuroinflammation 16:74.

Dulken BW, et al. (2019) Single-cell analysis reveals T-cell infiltration in old neurogenic niches. Nature 571:205–210.

Duscha A, et al. (2020) Propionic acid shapes the multiple sclerosis disease course by an immunomodulatory mechanism. Cell 180:1067–1080.e16.

Ferreiro AL, et al. (2023) Gut microbiome composition may be an indicator of preclinical Alzheimer's disease. Sci Transl Med 15:eabo2984.

Ferretti MT, Merlini M, Späni C, Gericke C, Schweizer N, Enzmann G, Engelhardt B, Kulic L, Suter T, Nitsch RM (2016) T-cell brain infiltration and immature antigen-presenting cells in transgenic models of Alzheimer's disease-like cerebral amyloidosis. Brain Behav Immun 54:211–225.

Forsythe P, Bienenstock J, Kunze WA (2014) Vagal pathways for microbiome-brain-gut axis communication. Adv Exp Med Biol 817:115–133.

Frost G, et al. (2014) The short-chain fatty acid acetate reduces appetite via a central homeostatic mechanism. Nat Commun 5:3611.

Furusawa Y, et al. (2013) Commensal microbe-derived butyrate induces the differentiation of colonic regulatory T cells. Nature 504:446–450.

Gate D, et al. (2020) Clonally expanded CD8 T cells patrol the cerebrospinal fluid in Alzheimer's disease. Nature 577:399–404.

Goehler LE, Gaykema RP, Opitz N, Reddaway R, Badr N, Lyte M (2005) Activation in vagal afferents and central autonomic pathways: early responses to intestinal infection with *Campylobacter jejuni*. Brain Behav Immun 19:334–344.

Gosselin D, et al. (2017) An environment-dependent transcriptional network specifies human microglia identity. Science 356:eaal3222.

Grubman A, et al. (2021) Transcriptional signature in microglia associated with Aβ plaque phagocytosis. Nat Commun 12:3015.

Hansen DV, Hanson JE, Sheng M (2018) Microglia in Alzheimer's disease. J Cell Biol 217:459–472.

Harach T, et al. (2017) Reduction of Abeta amyloid pathology in APPPS1 transgenic mice in the absence of gut microbiota. Sci Rep 7:41802.

Heneka MT, et al. (2015a) Neuroinflammation in Alzheimer's disease. Lancet Neurol 14:388–405.

Heneka MT, Golenbock DT, Latz E (2015b) Innate immunity in Alzheimer's disease. Nat Immunol 16:229–236.

Heyser CJ, Chemero A (2012) Novel object exploration in mice: not all objects are created equal. Behav Processes 89:232–238.

Jama HA, et al. (2020) Manipulation of the gut microbiota by the use of prebiotic fibre does not override a genetic predisposition to heart failure. Sci Rep 10:17919.

Jarry U, Jeannin P, Pineau L, Donnou S, Delneste Y, Couez D (2013) Efficiently stimulated adult microglia cross-prime naive $CD8^+$ T cells injected in the brain. Eur J Immunol 43:1173–1184.

Jiang Y, Li K, Li X, Xu L, Yang Z (2021) Sodium butyrate ameliorates the impairment of synaptic plasticity by inhibiting the neuroinflammation in 5XFAD mice. Chem Biol Interact 341:109452.

Kadowaki A, Quintana FJ (2020) The gut-CNS axis in multiple sclerosis. Trends Neurosci 43:622–634.

Kaye DM, et al. (2020) Deficiency of prebiotic fiber and insufficient signaling through gut metabolite-sensing receptors leads to cardiovascular disease. Circulation 141:1393–1403.

Keren-Shaul H, et al. (2017) A unique microglia type associated with restricting development of Alzheimer's disease. Cell 169:1276–1290.e17.

Kim HJ, Leeds P, Chuang DM (2009) The HDAC inhibitor, sodium butyrate, stimulates neurogenesis in the ischemic brain. J Neurochem 110:1226–1240.

Kimura I, et al. (2020) Maternal gut microbiota in pregnancy influences offspring metabolic phenotype in mice. Science 367:eaaw8429.

Koh A, De Vadder F, Kovatcheva-Datchary P, Bäckhed F (2016) From dietary fiber to host physiology: short-chain fatty acids as key bacterial metabolites. Cell 165:1332–1345.

Kundu P, et al. (2019) Neurogenesis and prolongevity signaling in young germ-free mice transplanted with the gut microbiota of old mice. Sci Transl Med 11:eaau4760.

Kurosawa T, Tega Y, Higuchi K, Yamaguchi T, Nakakura T, Mochizuki T, Kusuhara H, Kawabata K, Deguchi Y (2018) Expression and functional characterization of drug transporters in brain microvascular endothelial cells derived from human induced pluripotent stem cells. Mol Pharm 15:5546–5555.

Laurent C, et al. (2017) Hippocampal T-cell infiltration promotes neuroinflammation and cognitive decline in a mouse model of tauopathy. Brain 140:184–200.

Leger M, Quiedeville A, Bouet V, Haelewyn B, Boulouard M, Schumann-Bard P, Freret T (2013) Object recognition test in mice. Nat Protoc 8:2531–2537.

Li YJ, et al. (2020) Dietary fiber protects against diabetic nephropathy through short-chain fatty acid–mediated activation of G protein–coupled receptors GPR43 and GPR109A. J Am Soc Nephrol 31:1267–1281.

Long JM, Holtzman DM (2019) Alzheimer disease: an update on pathobiology and treatment strategies. Cell 179:312–339.

Lopez OL, Kuller LH (2019) Epidemiology of aging and associated cognitive disorders: prevalence and incidence of Alzheimer's disease and other dementias. Handb Clin Neurol 167:139–148.

Lourenco MV, et al. (2019) Exercise-linked FNDC5/irisin rescues synaptic plasticity and memory defects in Alzheimer's models. Nat Med 25:165–175.

Lourida I, Soni M, Thompson-Coon J, Purandare N, Lang IA, Ukoumunne OC, Llewellyn DJ (2013) Mediterranean diet, cognitive function, and dementia: a systematic review. Epidemiology 24:479–489.

Macia L, et al. (2015) Metabolite-sensing receptors GPR43 and GPR109A facilitate dietary fibre-induced gut homeostasis through regulation of the inflammasome. Nat Commun 6:6734.

Mariño E, et al. (2017a) Gut microbial metabolites limit the frequency of autoimmune T cells and protect against Type 1 diabetes. Nat Immunol 18:552–562.

Mariño E, et al. (2017b) Gut microbial metabolites limit the frequency of autoimmune T cells and protect against Type 1 diabetes. Nat Immunol 18:552–562.

Marques FZ, et al. (2017) High-fiber diet and acetate supplementation change the gut microbiota and prevent the development of hypertension and heart failure in hypertensive mice. Circulation 135:964–977.

Martorell AJ, et al. (2019) Multi-sensory gamma stimulation ameliorates Alzheimer's-associated pathology and improves cognition. Cell 177:256–271.e22.

Maslowski KM, et al. (2009) Regulation of inflammatory responses by gut microbiota and chemoattractant receptor GPR43. Nature 461:1282–1286.

Masters CL, Bateman R, Blennow K, Rowe CC, Sperling RA, Cummings JL (2015) Alzheimer's disease. Nat Rev 1:15056.

McAvoy KM, et al. (2016) Modulating neuronal competition dynamics in the dentate gyrus to rejuvenate aging memory circuits. Neuron 91:1356–1373.

Meyers EA, Gobeske KT, Bond AM, Jarrett JC, Peng CY, Kessler JA (2016) Increased bone morphogenetic protein signaling contributes to age-related declines in neurogenesis and cognition. Neurobiol Aging 38:164–175.

Morris MC, Tangney CC, Wang Y, Sacks FM, Bennett DA, Aggarwal NT (2015) MIND diet associated with reduced incidence of Alzheimer's disease. Alzheimers Dement 11:1007–1014.

Moseman E, Blanchard AC, Nayak D, McGavern DB (2020) T cell engagement of cross-presenting microglia protects the brain from a nasal virus infection. Sci Immunol 5:eabb1817.

Oakley H, Cole SL, Logan S, Maus E, Shao P, Craft J, Guillozet-Bongaarts A, Ohno M, Disterhoft J, Van Eldik L, Berry R, Vassar R (2006) Intraneuronal beta-amyloid aggregates, neurodegeneration, and neuron loss in transgenic mice with five familial Alzheimer's disease mutations: potential factors in amyloid plaque formation. J Neurosci 26:10129–10140.

Olson CA, Vuong HE, Yano JM, Liang QY, Nusbaum DJ, Hsiao EY (2018) The gut microbiota mediates the anti-seizure effects of the ketogenic diet. Cell 174:497.

Pasciuto E, et al. (2020) Microglia require CD4 T cells to complete the fetal-to-adult transition. Cell 182:625–640.e24.

Sampson TR, et al. (2016) Gut microbiota regulate motor deficits and neuroinflammation in a model of Parkinson's disease. Cell 167:1469–1480.e12.

Sharon G, et al. (2019) Human gut microbiota from autism spectrum disorder promote behavioral symptoms in mice. Cell 177:1600–1618.e17.

Smilowitz JT, O'Sullivan A, Barile D, German JB, Lönnerdal B, Slupsky CM (2013) The human milk metabolome reveals diverse oligosaccharide profiles. J Nutr 143:1709–1718.

Stinson LF, Gay MC, Koleva PT, Eggesbø M, Johnson CC, Wegienka G, du Toit E, Shimojo N, Munblit D, Campbell DE, Prescott SL, Geddes DT, Kozyrskyj AL (2020) Human milk from atopic mothers has lower levels of short chain fatty acids. Front Immunol 11:1427.

Streit WJ, Khoshbouei H, Bechmann I (2021) The role of microglia in sporadic Alzheimer's disease. J Alzheimers Dis 79:961–968.

Suarez AN, Hsu TM, Liu CM, Noble EE, Cortella AM, Nakamoto EM, Hahn JD, de Lartigue G, Kanoski SE (2018) Gut vagal sensory signaling regulates hippocampus function through multi-order pathways. Nat Commun 9:2181.

Tan J, McKenzie C, Vuillermin PJ, Goverse G, Vinuesa CG, Mebius RE, Macia L, Mackay CR (2016) Dietary fiber and bacterial SCFA enhance oral tolerance and protect against food allergy through diverse cellular pathways. Cell Rep 15:2809–2824.

Tan J, McKenzie C, Mariño E, Macia L, Mackay CR (2017) Metabolite-sensing G protein–coupled receptors: facilitators of diet-related immune regulation. Annu Rev Immunol 35:371–402.

Thompson LR, et al. Earth Microbiome Project Consortium (2017) A communal catalogue reveals earth's multiscale microbial diversity. Nature 551:457–463.

Thorburn AN, Macia L, Mackay CR (2014) Diet, metabolites, and 'Western-lifestyle' inflammatory diseases. Immunity 40:833–842.

Thorburn AN, et al. (2015) Evidence that asthma is a developmental origin disease influenced by maternal diet and bacterial metabolites. Nat Commun 6:7320.

Trompette A, et al. (2014) Gut microbiota metabolism of dietary fiber influences allergic airway disease and hematopoiesis. Nat Med 20:159–166.

Vailati-Riboni M, Rund L, Caetano-Silva ME, Hutchinson NT, Wang SS, Soto-Díaz K, Woods JA, Steelman AJ, Johnson RW (2022) Dietary fiber as a counterbalance to age-related microglial cell dysfunction. Front Nutr 9:835824.

van de Rest O, Berendsen AA, Haveman-Nies A, de Groot LC (2015) Dietary patterns, cognitive decline, and dementia: a systematic review. Adv Nutr 6:154–168.

Vijay N, Morris ME (2014) Role of monocarboxylate transporters in drug delivery to the brain. Curr Pharm Des 20:1487–1498.

Vogt NM, et al. (2017) Gut microbiome alterations in Alzheimer's disease. Sci Rep 7:13537.

Yap YA, et al. (2021) An acetate-yielding diet imprints an immune and anti-microbial programme against enteric infection. Clin Transl Immunol 10:e1233.

Yu L, Zhong X, He Y, Shi Y (2020) Butyrate, but not propionate, reverses maternal diet-induced neurocognitive deficits in offspring. Pharmacol Res 160:105082.

Yuan P, Condello C, Keene CD, Wang Y, Bird TD, Paul SM, Luo W, Colonna M, Baddeley D, Grutzendler J (2016) TREM2 haplodeficiency in mice and humans impairs the microglia barrier function leading to decreased amyloid compaction and severe axonal dystrophy. Neuron 90:724–739.